# **Multi-Objective Bilevel Learning**

# Zhiyao Zhang<sup>1</sup>, Zhuqing Liu<sup>2</sup>, Xin Zhang<sup>3</sup>, Wen-Yen Chen<sup>3</sup>, Jiyan Yang<sup>3</sup>, Jia Liu<sup>1</sup>

<sup>1</sup>Dept. of Electrical and Computer Engineering, The Ohio State University <sup>2</sup>Dept. of Computer Science, University of North Texas <sup>3</sup>Meta Platforms, Inc.

#### Abstract

As machine learning (ML) applications grow increasingly complex in recent years, modern ML frameworks often need to address multiple potentially conflicting objectives with coupled decision variables across different layers. This creates a compelling need for multi-objective bilevel learning (MOBL). So far, however, the field of MOBL remains in its infancy and many important problems remain under-explored. This motivates us to fill this gap and systematically investigate the theoretical and algorithmic foundation of MOBL. Specifically, we consider MOBL problems with multiple conflicting objectives guided by preferences at the upper-level subproblem, where part of the inputs depend on the optimal solution of the lower-level subproblem. Our goal is to develop efficient MOBL optimization algorithms to (1) identify a preferenceguided Pareto-stationary solution with low oracle complexity; and (2) enable systematic Pareto front exploration. To this end, we propose a unifying algorithmic framework called weighted-Chebyshev multi-hyper-gradient-descent (WC-MHGD) for both deterministic and stochastic settings with finite-time Pareto-stationarity convergence rate guarantees, which not only implies low oracle complexity but also induces systematic Pareto front exploration. We further conduct extensive experiments to confirm our theoretical results.

### 1 Introduction

1) Background and motivation: As machine learning (ML) applications grow increasingly complex, modern ML training frameworks often need to address multiple objectives that are potentially conflicting. As an example, in the design of online shopping recommender systems, the objective of a training loss function could aim to prioritize lower prices, more popular brand names, or faster delivery speeds, all of which may be in conflict with each other. Moreover, such objective functions could further depend on an optimal solution from a separate and coupled optimization task, thus making the overall training task bilevel in nature. For instance, the multiobjective trainings in the aforementioned online shopping recommender system could all rely on a joint pre-training of a set of shared model parameters that define all objectives. Similar multi-objective bilevel problem structures also arise from multi-agent reinforcement learning with an actor-critic

Copyright © 2026, Association for the Advancement of Artificial Intelligence (www.aaai.org). All rights reserved.

framework (Ji, Yang, and Liang 2021; Yang, Ji, and Liang 2021; Zhang et al. 2024; Qiu et al. 2023) and the pretraining-finetuning pipeline of multi-task adaptation of a foundation model (Chakraborty et al. 2024; Shen, Yang, and Chen 2024). These complex problem structures create a compelling need for multi-objective bilevel learning (MOBL).

Mathematically, an MOBL problem can be formulated in the following general form:

$$\min_{x \in \mathbb{R}^p} \Phi(x) := [\phi_1(x), \dots, \phi_S(x)]$$
s.t.  $y^*(x) \in \underset{y \in \mathbb{R}^q}{\arg \min} g(x, y),$  (1)

where  $\phi_s(x) := f^{(s)}(x, y^*(x)), s \in [S]$ , represents an upperlevel (UL) objective function with an implicit UL decision variable  $y^*(x)$  being an optimizer of a lower-level (LL) subproblem. Clearly, MOBL combines the problem structures of multi-objective optimization (MOO) and bilevel optimization (BLO), both of which are challenging ML optimization paradigms in their own right and have attracted a significant amount of attention in the research community in recent years. Although numerous algorithms have been proposed for solving MOO and BLO problems (e.g., (Konak, Coit, and Smith 2006; Sener and Koltun 2018; Yang et al. 2024a) for MOO and (Ji, Yang, and Liang 2021; Yang, Ji, and Liang 2021; Zhang et al. 2024; Qiu et al. 2023) for BLO, respectively; see Section 2 for in-depth discussions), the field of MOBL remains in its infancy, with many important open problems yet to be addressed. This gap between current MOBL research state and practical needs of MOBL arises primarily from the following technical challenges.

2) Technical challenges: Solving MOBL problems is, surprisingly, significantly more challenging than a straightforward combination of applying existing MOO and BLO solution techniques, which is due to the following two key factors: First, being both multi-objective and bilevel, an MOBL problem not only inherits all the challenges of MOO and BLO, but also sees many unique and new complications unseen in either MOO or BLO. Specifically, due to the finite-time constraint in solving the LL problem under the bilevel structure of MOBL problems, one typically has an inexact  $y_k$  at each iteration instead of the true solution  $y^*(x_k)$ . This inaccuracy in  $y_k$  subsequently results in a biased estimate  $\hat{\nabla}\phi_s(x_k)$ , which could deviate from a common descent direction computed according to  $\nabla\phi_s(x_k)$  for all objectives.

Beyond the cascaded error in  $\nabla \phi_s(x_k)$ , the inaccuracy can accumulate over iterations, causing the solution trajectory to drift significantly from the desired target. Second, preference-guided Pareto front (i.e., the set of all Pareto-optimal solutions) exploration in MOBL is even more challenging (see solution philosophies in Section 3 for more details), since the Pareto stationarity (necessary condition of Pareto-optimality) and preference alignment should be balanced in the algorithmic design, which is highly susceptible to the accumulative cascaded errors inherent in the bilevel structure. Moreover, although existing works have incorporated scalarization methods to handle preference alignment, conventional rescaling strategies no longer apply due to the bilevel nature of MOBL problems, thereby necessitating novel technical designs.

- 3) Main contributions: In this paper, we propose a series of new MOBL algorithms to overcome the aforementioned challenges, all of which enjoy a fast finite-time convergence rate guarantees and hence low oracle complexities. Collectively, our results contribute toward establishing a theoretical foundation for MOBL. Our main contributions and key results are summarized as follows:
  - We propose a unifying MOBL algorithmic framework called weighted-Chebyshev multi-hyper-gradient-descent (WC-MHGD) for both deterministic and stochastic settings. Our WC-MHGD framework offers provable fast finite-time convergence rates and low oracle complexities of  $\mathcal{O}(\epsilon^{-1})$  and  $\mathcal{O}(\epsilon^{-2})$  for achieving an  $\epsilon$ -Pareto stationary solution in deterministic and stochastic settings, respectively. To our knowledge, our finite-time convergence and oracle complexity results are the first of their kind in the MOBL literature involving preference.
- It is worth pointing out that the algorithmic design and theoretical convergence analysis of our proposed WC-MHGD framework are highly non-trivial and far from straightforward extensions of traditional MOO and BLO techniques. Notably, we rigorously show that our *new* dynamic weighting optimization subproblem (cf. Eq. (5)) guarantees Pareto stationarity in MOBL problems. Moreover, we establish a general result that the preference-guided dynamic weighted hypergradient direction in WC-MHGD satisfies a key minimum-norm condition (cf. Lemma 5.4), which serves as a foundation for our theoretical analysis and could be of independent interest for other MOBL research problems.
- In addition to WC-MHGD algorithmic design and theoretical convergence analysis, we also offer the rationale behind our key algorithmic approaches and the geometric interpretation of our WC-MHGD approach in this paper, which advances and deepens our fundamental understandings of MOBL optimization theory and algorithms. Moreover, in Section 6, we conduct extensive numerical experiments to verify our WC-MHGD algorithms. All of our empirical results confirm the efficacy and effectiveness of our WC-MHGD algorithms.

### 2 Related Work

In this section, we provide an overview on recent works in MOBL to put our work in comparative perspectives. Due

to space limitation, we relegate the overview of two closely related research areas, namely multi-objective optimization and bilevel optimization to Appendix B.

As mentioned in Section 1, the field of MOBL remains in a nascent stage and results in this area are rather limited. To our knowledge, existing works on MOBL include (Wang, Singh, and Ray 2024; Li et al. 2024; Yang et al. 2024b; Ye et al. 2024, 2021; Gu et al. 2023). Among these, the MOBL algorithms proposed in (Wang, Singh, and Ray 2024; Li et al. 2024) only provided empirical results without theoretical convergence and oracle complexity analysis. In contrast, it was shown that algorithms in (Yang et al. 2024b; Ye et al. 2021) converge to a Pareto stationary point. However, no finite-time convergence rate result was provided.

The most related works to our paper are (Ye et al. 2024; Fernando et al. 2022), which have been shown to offer a finitetime convergence rate for the deterministic and stochastic setting, respectively. However, our work differs from (Fernando et al. 2022; Ye et al. 2024) in the following key aspects: (1) Due to the use of less efficient value function algorithmic approach, the convergence rates in (Fernando et al. 2022; Ye et al. 2024) are  $\mathcal{O}(SK^{-\frac{1}{2}})$  and  $\mathcal{O}(1/K^{\frac{1}{4}})$ , respectively. In contrast, with a judicious algorithmic design, our WC-MHGD approach achieves a significantly faster  $\mathcal{O}(1/K)$ finite-time convergence rate, and covers both the deterministic setting and the stochastic setting simultaneously; and (2) Our WC-MHGD approach enables a systematic *Pareto* stationarity front exploration guided by preferences (see solution philosophies in Section 3 for more details). Due to space limitation, we provide a detailed comparison in Appendix B.

### 3 Multi-Objective Bilevel Learning: A Primer

To facilitate our MOBL deterministic and stochastic algorithm designs and theoretical convergence analysis, we first provide a primer on MOBL in this section.

1) Deterministic and Stochastic Versions of MOBL: Note that the deterministic version of the MOBL problem is stated Eq. (1) in Section 1. For the stochastic version of the MOBL problem, we assume the UL and LL objective functions can be expressed in the following forms, respectively:

$$\phi_s(x) = f^{(s)}(x, y^*(x)) := \mathbb{E}_{\xi \sim \pi_s}[F^{(s)}(x, y^*(x); \xi)],$$
  
$$g(x, y) := \mathbb{E}_{\zeta \sim \pi_s}[G(x, y; \zeta)],$$

where  $\pi_s$  and  $\pi_g$  represent the data distributions underlying the s-th UL and the LL objective functions, respectively. As will be shown later, the deterministic and stochastic versions of MOBL will have key differences in their algorithmic designs and theoretical convergence analysis.

2) Optimality Criterion of MOBL: As mentioned in Section 1, it is in general impossible to find a common x-solution to minimize all UL functions simultaneously due to the presence of potential conflicts between them. As a result, it is more appropriate to adopt the following notion of Pareto optimality as the performance metric for MOBL:

**Definition 3.1** (Pareto Optimality). A solution  $x_1$  is said to dominate another solution  $x_2$  if and only if 1)  $\phi_s(x_1) \le \phi_s(x_2)$ ,  $\forall s \in [S]$  and 2) there exists at least one  $s \in [S]$ 

such that the inequality holds strictly. A solution x is Pareto optimal if no other  $x^\prime$  dominates x.

Similar to solving most non-convex MOO or BLO problems, finding a Pareto-optimal solution in non-convex MOBL is NP-Hard in general. As a result, it is often more practical to search for a Pareto-stationary solution defined as follows (a necessary condition for Pareto optimality):

**Definition 3.2** (Pareto Stationarity). A solution x is Pareto stationary if there does not exist a common descent direction  $d \in \mathbb{R}^p$  such that  $\nabla \phi_s(x)^{\top} d < 0, \forall s \in [S]$ .

Although Definition 3.2 rigorously defines the notion of Pareto stationary solution, it is inconvenient to work with in MOBL algorithm design. Toward this end, we will adopt the notion of  $\epsilon$ -Pareto stationary solution defined as follows:

**Definition 3.3** ( $\epsilon$ -Pareto Stationarity). Let  $\nabla \Phi(x) := [\nabla \phi_1(x), \dots, \nabla \phi_S(x)]^{\top}$ . A solution x is  $\epsilon$ -Pareto stationary if, for  $\epsilon > 0$ , there exists a vector  $\lambda \in \mathbb{R}^S$  in the S-simplex (i.e.,  $\lambda$  is nonnegative and  $\mathbf{1}^{\top}\lambda = 1$ ) such that the  $\lambda$ -weighted gradient direction  $d := \nabla \Phi(x)\lambda \in \mathbb{R}^p$  satisfies  $\|d\|^2 \leq \epsilon$ .

The above  $\epsilon$ -Pareto stationarity is derived from solving the Lagrangian dual problem of minimizing the worst descent among all UL objectives, which is logically equivalent to Definition 3.1 (cf. e.g., (Sener and Koltun 2018; Yang et al. 2024a; Zhou et al. 2024)). We note that Definition 3.3 not only provides a useful metric in convergence analysis, but also motivates our WC-MHGD algorithm design later.

- 3) MOBL Solution Philosophies: Due to the flexible multi-objective nature of MOBL problems, there are four basic solution philosophies commonly seen in practice, depending on whether or not a preference weight vector  $r \in \Delta_S^+$  (S-simplex) associated with the UL objectives is used:
- **P1**) Given preference r, identify a Pareto stationary point that aligns most closely with the preference;
- **P2**) Explore (partially) the Pareto front first, and then allow the decision-maker to select one from the exploration results based on some given preference r;
- **P3**) Allow the decision-maker to select iteratively by combining 1) and 2) with changing preferences;
- **P4**) Identify a solution based on certain global criterion rather than relying on preference information.

In this paper, we focus on Philosophy **P2**, since (i) the preference weight r could be difficult to pre-determine in many MOBL applications; and (ii) the preference vector r may not intersect with the Pareto front, rendering the P1 problem ill-defined. Also, we will show in Section 5 that the P4 can be treated as a *special case* of our proposed solution.

Under Philosophy P2, our goal in solving a non-convex MOBL problem is two-fold: (1) achieving a  $\epsilon$ -Pareto stationary solution; and (2) systematically exploring the Pareto-stationarity front (i.e., the collection of all Pareto-stationary solutions) guided by preference information.

### 4 The Proposed WC-MHGD Algorithms

In this section, we will first provide necessary preliminaries of our algorithmic designs in Section 4.1. Then, we will present our WC-MHGD algorithms for deterministic and stochastic settings in Sections 4.2 and 4.3, respectively.

#### 4.1 Preliminaries

1) The basic idea of our WC-MHGD algorithms: To achieve our first goal in finding a Pareto stationary solution in MOBL, our idea is to generalize the multi-gradient descent algorithm (MGDA) (Désidéri 2012) for solving MOO problems (Coello 2007; Elsken, Metzen, and Hutter 2018; Xu et al. 2024; Sener and Koltun 2018) by replacing gradient information in MGDA with the hypergradient used in BLO approaches, hence the name multi-hypergradient-descent (MHGD). Specifically, MHGD can be viewed as an extension of the (stochastic) gradient descent method to the multiobjective bilevel setting by first identifying a common UL descent direction that reduces the values of all S UL objectives, and then move along this direction with an appropriately chosen step-size. If no common descent direction exists, then the current solution is a Pareto stationary point of the UL subproblem.

Next, to achieve the second goal in systematic Paretostationarity front exploration, we propose to integrate the weighted Chebyshev (WC) scalarization technique with our MHGD design. The WC-scalarization transforms a vector-valued objective function into a scalar-valued objective function, which is more amenable for algorithm design. Specifically, let  $\Delta_S^+$  represent the S-dimensional simplex. In an MOBL problem, the WC-scalarization with a preference vector  $r \in \Delta_S^+$  is defined in the following  $\min$ -max form:  $\operatorname{WC}_r(\Phi(x)) := \min_x \max_i \{r_i \phi_i(x)\}_{i=1}^S = \min_x \|r \odot \Phi(x)\|_{\infty}$ , where  $\odot$  denotes the Hadamard product. The use of WC-scalarization in our WC-MHGD algorithmic design is motivated by the following key fact in MOO (Golovin and Zhang 2020; Qiu et al. 2024):

**Lemma 4.1** (Pareto Optimality Equivalence). A solution  $x^*$  is weakly Pareto-optimal to an MOO problem  $\min_x \Phi(x)$  if and only if  $x^* \in \arg\min_x \mathsf{WC}_r(\Phi(x))$  for some  $r \in \Delta_S^+$ .

Lemma 4.1 suggests that, by appropriately integrating WC-scalarization in MOBL algorithm design, we can systematically obtain all weakly Pareto-optimal solutions (i.e., exploring the weak Pareto front) by enumerating the WC-scalarization preference weight vector  $\boldsymbol{r}$  if the WC-scalarization problem can be solved optimally. Indeed, combining the WC scalarization and MHGD yields our WC-MHGD framework.

2) The hypergradient of the MOBL problem: In our WC-MHGD algorithms, we need to evaluate the set of all hypergradients denoted by the matrix  $\nabla\Phi(x)$ , or equivalently, to find the hypergradient  $\nabla\phi_s(x)$  of each UL objective  $s\in[S]$ . Following the implicit function theorem (Zhang et al. 2024), it can be shown that the each UL hypergradient can be computed as follows (Ghadimi and Wang 2018; Ji, Yang, and Liang 2021):

$$\nabla \phi_s(x) = \nabla_x f^{(s)}(x, y^*(x)) - \nabla_{xy}^2 g(x, y^*(x)) v^*, \quad (2)$$

where  $v^*$  is the solution of the following linear equation system  $\nabla_y^2 g(x,y^*(x))v = \nabla_y f^{(s)}(x,y^*(x))$ . It is clear from Eq. (2) and the definition of  $v^*$  that the Hessian  $\nabla_y^2 g(x,y^*(x))$  being invertible is a *necessary* condition for the hypergradient  $\phi_s(x)$  to be well-defined. Similar to most

existing works on bilevel optimization in the ML literature, in this paper, we assume that the LL function g(x,y) is strongly convex in y (cf. Theorem 5.1), so that  $\nabla^2_y g(x,y^*(x))$  is positive definite and hence invertible. Thus, the LL solution  $y^*(x)$  can be uniquely determined.

In practice, however, since the LL subproblem is typically solved numerically, one usually does *not* have the exact  $y^*(x)$ -solution and can only use some estimation of  $y^*(x)$  in Eq. (2) to compute the hypergradient. Consequently, the inexact  $y^*(x)$ -information results in systematic bias in hypergradient information. Indeed, most of our subsequent MOBL algorithm designs in deterministic and stochastic settings are centered around addressing this key challenge.

Moreover, note that the hypergradient evaluation in Eq. (2) involves numerous first-order and second-order oracle evaluations (i.e., the gradient information, the Jacobian information, and the Hessian information), all of which are computationally expensive. Therefore, to evaluate the efficiency of our proposed algorithms, we adopt the *oracle complexity* metric (Zhang et al. 2024). Specifically, we let  $\mathrm{Gc}(f^{(s)},\epsilon)$  denote the number of the first-order oracle evaluations (i.e., partial gradients  $\nabla_x f^{(s)}$  and  $\nabla_y f^{(s)}$ ) for  $f^{(s)}(x,y)$ ,  $s \in [S]$ . Also, for a vector v and a positive  $\epsilon$ , we let  $\mathrm{JV}(g,\epsilon)$  and  $\mathrm{HV}(g,\epsilon)$  represent the numbers of second-order oracle evaluations in Jacobian-vector product  $\nabla^2_{xy} g(x,y) v$  and Hessian-vector product  $\nabla^2_y g(x,y) v$ , respectively. Then, the oracle complexity is defined as follows:

**Definition 4.2** (Oracle Complexity of MOBL Algorithms). The oracle complexity of an MOBL algorithm is defined as the total required numbers of first-order and second-order oracle evaluations for the algorithm to converge to an  $\epsilon$ -Paretostationary solution.

With all these preliminaries, we are now in a position to present our WC-MHGD algorithms.

#### 4.2 The Deterministic WC-MHGD Algorithm

As illustrated in Algorithm 1, our deterministic WC-MHGD algorithm adopts a "double-loop" structure. In the inner-loop, we perform gradient-descent-style updates to approximately find the optimal  $y^*(x_k)$ -solution in the k-th outer iteration. To accelerate convergence, we apply a "warm start" technique inspired by (Ji, Yang, and Liang 2021): the output from the end of the previous round of inner iterations serves as the initial point for the current round of inner iterations. After D inner iterations,  $y_k^D$  will be used as an estimation of  $y^*(x_k)$ . In the k-th iteration of the outer-loop, we offer two options to compute the hypergradient for each UL objective  $s \in [S]$ . Option 1 performs N steps of the conjugate-gradient method (CG) to solve the linear equation system  $\nabla_y^2 g(x_k, y_k^D) v = \nabla_y f^{(s)}(x_k, y_k^D)$  to obtain  $v_k^{(s),N}$ , which is used to compute the hypergradient as:

$$\hat{\nabla}\phi_s(x_k) = \nabla_x f^{(s)}(x_k, y_k^D) - \nabla_{xy}^2 g(x_k, y_k^D) v_k^{(s), N}.$$
 (3)

In comparison, Option 2 approximates the Hessian inverse with the Neumann series  $[\nabla_y^2 g(x_k,y_k^D)]^{-1} \approx \prod_{j=t+1}^{D-1} (I-1)^{-1}$ 

Algorithm 1: Deterministic WC-MHGD.

```
1: Input: The numbers of iteration K, D, N, initialization
      values x_0, y_0, v_0, preference r, and step-sizes \alpha, \beta.
 2: for k = 0, 1, ..., K - 1 do

3: Set y_k^0 = y_{k-1}^D if k > 0 and y_0 otherwise.

4: for t = 1, 2, ..., D do

5: Update y_k^t = y_k^{t-1} - \alpha \nabla_y g(x_k, y_k^{t-1}).
 6:
 7:
         for s \in [S] do
 8:
             Option 1: Conjugate-Gradient(CG)
             Set v_k^{(s),0} = v_{k-1}^{(s),N} if k > 0 and v_0 otherwise.
 9:
            Solve \nabla_y^2 g(x_k, y_k^D) v = \nabla_y f^{(s)}(x_k, y_k^D) for N steps from v_k^{(s),0} to get v_k^{(s),N}.
10:
             Compute \hat{\nabla}\phi_s(x_k) according to Eq. (3).
11:
             Option 2: Neumann-Series(NS)
12:
13:
             Compute \nabla \phi_s(x_k) according to Eq. (4).
14:
15:
         Compute \lambda_k according to Equation (5).
         Update x_{k+1} = x_k - \beta \hat{\nabla} \Phi(x_k) (r \odot \lambda_k).
17: end for
```

 $\nabla_y^2 g(x_k, y_k^j)$ ) and compute the hypergradient as:

$$\hat{\nabla}\phi_{s}(x_{k}) = \nabla_{x}f^{(s)}(x_{k}, y_{k}^{D}) - \alpha \sum_{t=0}^{D} \nabla_{xy}^{2}g(x_{k}, y_{k}^{t})$$

$$\prod_{j=t+1}^{D-1} (I - \nabla_{y}^{2}g(x_{k}, y_{k}^{j}))\nabla_{y}f^{(s)}(x_{k}, y_{k}^{D}).$$
(4)

With the hypergradients obtained from Eqs. (3) or (4), the heart of our WC-MHGD algorithm is to solve the following convex quadratic programming problem to find the optimal  $\lambda$ -weights to linearly combine hypergradients:

$$\min_{\lambda \ge \mathbf{0}} \underbrace{\|K(r \odot \lambda)\|]^2}_{\text{MHGD}} - u \underbrace{\lambda^{\top}(r \odot \Phi(x_k))}_{\text{WC-Scalarization}}$$
s.t.  $\mathbf{1}^{\top} \lambda = 1$ . (5)

where u>0 is a tunable parameter, and  $K:=(\hat{\nabla}\Phi(x_k)^{\top}\hat{\nabla}\Phi(x_k))^{\frac{1}{2}}\in\mathbb{R}^{S\times S}$ . Upon obtaining  $\lambda_k^u$  by solving Problem (5), we compute the update direction  $d_k(u)$  by taking the gradient of the Lagrangian of Problem (5) to yield  $d_k(u)=\hat{\nabla}\Phi(x_k)(r\odot\lambda_k^u)$ . For brevity, we will simply denote  $\lambda_k^u$  and  $d_k(u)$  as  $\lambda_k$  and  $d_k$ , respectively, when the context is clear. Three important remarks are in order on Problem (5), which is a **new design** unseen in the literature:

1) The first term in Problem (5) plays the role of searching for a Pareto-stationary solution. To see this, it is insightful to recognize that the first term  $\|K(r\odot\lambda)\|^2$  in Problem (5) is equivalent to  $\|\hat{\nabla}\Phi(x_k)(r\odot\lambda)\|^2$  in the k-th iteration (it is advantageous to use K instead of  $\hat{\nabla}\Phi(x_k)$  since the dimension of K is typically much smaller  $(S\ll p)$ ). Consequently,  $\|K(r\odot\lambda)\|^2 = \|\hat{\nabla}\Phi(x_k)\mathrm{diag}(r)\lambda\|^2$ , where  $\mathrm{diag}(r)$  denotes the diagonal matrix with elements in r on the main diagonal.  $\|K(r\odot\lambda)\|^2$  can be viewed as an r-scaled version

#### Algorithm 2: Stochastic WC-MHGD

```
1: Input: The numbers of iteration K, D, Q, initialization
        values x_0, y_0, preference r, and step-sizes \alpha, \beta.
 2: for k=0,1,\ldots,K do
3: Set y_k^0=y_{k-1}^D if k>0 and y_0 otherwise.
4: for t=1,2,\ldots,D do
5: Draw a sample batch \mathcal{T}_{t-1}, and update y_k^t=y_k^{t-1}-\alpha\nabla_y G(x_k,y_k^{t-1};\mathcal{T}_{t-1}).
 6:
             Draw sample batches \mathcal{D}_G, \mathcal{D}_H.
 7:
 8:
             for s \in [S] do
 9:
                  Draw sample batch \mathcal{D}_F^s.
                 Set v_k^{(s),0} = \nabla_y F^{(s)}(x_k,y_k^D;\mathcal{D}_F^s).

Compute v_k^{(s),Q} via algorithm 3, and \hat{\nabla}\phi_s(x_k) = \nabla_x F^{(s)}(x_k,y_k^D;\mathcal{D}_F^s) - \nabla_{xy}^2 G(x_k,y_k^D;\mathcal{D}_G)v_k^{(s),Q}.
10:
11:
12:
             Compute \lambda_k according to Eq. (5).
13:
             Update x_{k+1} = x_k - \beta \hat{\nabla} \Phi(x_k) (r \odot \lambda_k).
14:
15: end for
```

of  $\|\hat{\nabla}\Phi(x_k)\lambda\|^2$ . Since r is strictly positive, the  $\lambda$ -vector that minimizes  $\|\hat{\nabla}\Phi(x_k)\lambda\|^2$  provides a **common descent direction**  $d=\hat{\nabla}\Phi(x_k)(r\odot\lambda)$  that improves all objectives. It is worth pointing out that the use of  $\|K(r\odot\lambda)\|^2$  instead of the quadratic term  $\|\Phi(x_k)\lambda\|^2$  in the original MGDA (Désidéri 2012) is **a major novelty** in this paper. Indeed, this above Pareto-stationarity intuition can be made rigorous and stated as follows (proved in Appendix D):

**Lemma 4.3** (Pareto Stationarity). For any preference  $r \in \mathbb{R}^S_{++}$ , if the first term in Eq. (5) satisfies  $K(r \odot \lambda) = 0$ , then Pareto stationarity is achieved.

- 2) The second term  $-\lambda^{\top}(r\odot\Phi(x_k))$  in Problem (5) is used to facilitate the WC-scalarization for systematic Pareto stationarity front exploration. To see why this term is corresponding to the WC scalarization, note that the primal WC problem can be written as minimizing a scalar  $\gamma$  subject to  $r\odot\Phi(x_k)\leq\gamma$ 1, which effectively minimizes the weighted loss in  $\ell_{\infty}$ -norm sense (Momma, Dong, and Liu 2022). Then, by taking the Wolfe dual to incorporate Paretostationarity conditions, this WC-related objective transforms into maximizing  $u\lambda^{\top}(r\odot\Phi(x_k))$ , or equivalently minimizing  $-u\lambda^{\top}(r\odot\Phi(x_k))$ .
- 3) By choosing an appropriate u-value, the objective function in Problem (5) strikes a balance between minimizing Pareto-stationarity gap under preference r and systematically explore Pareto-stationarity front following the r-weighted WC scalarization. Specifically, if Pareto-stationarity front exploration is of higher priority, one can choose a larger u-value. Otherwise, a small u-value favors minimizing the Pareto-stationarity gap of the obtained solution. Geometric insight of Problem (5) is provided in Appendix C due to space limitation.
- **4)** In addition to the new algorithmic design of Problem (5) (as shown in Theorem 5.4), we also emphasize that the overall framework design of WC-MHGD approach is a *consequence*

Algorithm 3: Hessian-vector Product  $v_k^{(s),Q}$  Computation

```
1: Input: The number of iteration Q, initialization values v_k^{(s),Q}, samples \mathcal{D}_H = \{\mathcal{B}_j\}_{j=1}^Q and step-sizes \eta.

2: for j=1,2,\ldots,Q do

3: Use \mathcal{B}_j to compute G_j(y)=y-\eta\nabla_yG(x,y;\mathcal{B}_j).

4: end for

5: Set \nu^{(s),Q}=v_k^{(s),0}.

6: for i=Q,Q-1,\ldots,1 do

7: Compute \nu^{(s),i-1}=\nu^{(s),i}-\eta\nabla_y^2G(x,y;\mathcal{B}_i)\nu^{(s),i}.

8: end for

9: Output: v_k^{(s),Q}=\eta\sum_{i=0}^Q\nu^{(s),i-1}.
```

of the special problem structure in MOBL. Specifically, we note that a family of BLO algorithms (namely SOBA-based approaches update UL and LL variables x and y simultaneously in each iteration, (Dagréou et al. 2022; Liu et al. 2023a)) achieves efficient convergence rate in the context of BLO. However, such SOBA-based approaches are not applicable in MOBL when multiple objectives are taken into account, since the v-variables lose their dual variable meaning as their counterpart in the single-objective setting. In contrast, our WC-MHGD method handles LL and UL variables in an alternating manner to avoid the explicit use of dual variables. This overcomes the limitation of the SOBA-based approaches and is specifically designed for MOBL problems.

### 4.3 The Stochastic WC-MHGD Algorithm

The stochastic WC-MHGD is illustrated in Algorithm 2, which shares a similar structure and is based on the same intuition as in Algorithm 1. The key differences of the stochastic WC-MHGD algorithm include: (1) In the t-th inner loop iteration, the y-updates are conducted in a stochastic gradient descent fashion with a sample batch  $\mathcal{T}_{t-1}$  and similar warm start technique as in deterministic WC-MHGD. (2) In the k-th outer loop iteration, the Hessian-vector product  $v_k^{(s),Q}$  required for hypergradient computation is inspired by (Ji, Yang, and Liang 2021), which also uses the Neumann series technique for Hessian inverse approximation as shown in Algorithm 3. However, the computation of  $v_k^{(s),Q}$  is significantly more complex compared to the deterministic case and care must be taken to tame oracle complexity. Similar to (Ji, Yang, and Liang 2021), we select mutually independent datasets  $\mathcal{B}_j$  with exponentially shrinking sizes in Algorithm 3.

## 5 Pareto-Stationarity Convergence Analysis

In this section, we start by introducing several assumptions required for our analysis, which are followed by the main finite-time convergence results of our WC-MHGD algorithms.

**Assumption 5.1** (LL Objective Function). For any  $x \in \mathbb{R}^p$ ,  $g(x,\cdot)$  in the deterministic setting and  $G(x,\cdot;\zeta)$  in the stochastic setting are  $\mu_g$ -strongly-convex with respect to y for some constant  $\mu_g > 0$ .

We note that Assumption 5.1 is standard and has been widely adopted in the literature (Ji, Yang, and Liang 2021; Yang, Ji, and Liang 2021; Liu et al. 2023b; Hu et al. 2023; Yang, Xiao,

and Ji 2023; Gong, Hao, and Liu 2024). On one hand, strong convexity ensures that the Hessian inverse  $\nabla_y^2 g(x,y)^{-1}$  well-defined and that the solution to the LL subproblem can be uniquely determined; on the other hand, it enables the quantification of the error between the approximated and ground-truth hypergradients.

**Assumption 5.2** (Smoothness). There exist positive constants M, L,  $\tau$ , and  $\rho$ , such that for any  $s \in [S]$  and any  $z, z' \in \mathbb{R}^{p+q}$ , the following Lipchitz continuity conditions hold under the deterministic setting:

$$\begin{split} |f^{(s)}(z) - f^{(s)}(z')| &\leq M \|z - z'\|, \\ \|\nabla f^{(s)}(z) - \nabla f^{(s)}(z')\| &\leq L \|z - z'\|, \\ \|\nabla g(z) - \nabla g(z')\| &\leq L \|z - z'\|, \\ \|\nabla_{xy}^2 g(z) - \nabla_{xy}^2 g(z')\| &\leq \tau \|z - z'\|, \\ \|\nabla_{y}^2 g(z) - \nabla_{y}^2 g(z')\| &\leq \rho \|z - z'\|, \end{split}$$

where  $\|\cdot\|$  denotes the  $\ell_2$ -induced norm (abbreviated as  $\|\cdot\|$  in the sequel for simplicity). In addition, the stochastic functions  $F^{(s)}(z;\xi)$  and  $G(z;\zeta)$  also satisfy their corresponding smoothness assumptions for any sample pairs  $\xi$  and  $\zeta$ .

We note that the above smoothness assumptions are also standard and have been widely adopted in the literature for convergence analysis (Ghadimi and Wang 2018; Ji, Yang, and Liang 2021; Qiu et al. 2023; Yang, Ji, and Liang 2021; Lin et al. 2024a). Lastly, we make the following assumption on the variance of the LL objective function as follows:

**Assumption 5.3** (Bounded LL Variance). The LL stochastic gradient  $\nabla G(z;\zeta)$  has a variance bounded by a constant  $\sigma>0$ , i.e.,  $\mathbb{E}_{\mathcal{L}}\|\nabla G(z;\zeta)-\nabla g(z)\|^2\leq\sigma^2$ .

1) Convergence Rate of the Deterministic WC-MHGD: We let  $\bar{d}_k = \nabla \Phi(x_k) \mathrm{diag}(r) \lambda_k$  for any  $k \in \{0,\dots,K\}$ . Also, we let  $\kappa = \frac{L}{\mu_g}$  denote the condition number and define  $L_\phi := L + \frac{2L^2 + \tau M^2}{\mu_g} + \frac{\rho L M + L^3 + \tau L M}{\mu_g^2} + \frac{\rho L^2 M}{\mu_g^3} = \Theta(\kappa^3)$ . We first state a key result to establish the convergence of our WC-MHGD method, which is new for MOBL problems and

not in the MOO and BLO literature.

**Lemma 5.4** (Preference-Guided Minimum-Norm Lemma). Let  $\lambda_k^u$  be obtained from solving Problem (5) for some u > 0 and thus the update direction is  $d_k(u) := \hat{\nabla} \Phi(x_k) (r \odot \lambda_k^u)$ . Let  $r_{max}$  be the maximal element of r. For any  $s \in [S]$  and  $r \in \Delta_S^+$ , there exists a sufficiently small u such that the following holds:  $\|d_k(u)\|^2 \leq 2r_{max}\langle d_k(u), \hat{\nabla} \phi_s(x_k) \rangle$ .

Theorem 5.4 plays an important role in the subsequent analysis. While the relationship between the derived direction  $d_k$  and the gradient  $\hat{\nabla}\phi_s(x_k)$  in MGDA is well understood, it only holds in conventional MOO settings. Therefore, adopting the newly designed Problem (5) is essential for MOBL problems. However, this new design also implies a *new* common descent direction  $d_k(u)$ , for which *no existing works* have characterized its properties. To this end, we establish Theorem 5.4 to reveal how  $d_k(u)$  correlates with r and  $\hat{\nabla}\phi_s$ . The result proved in Theorem 5.4 further leads to our finite-time convergence rate result, which is stated as follows:

**Theorem 5.5** (Finite-Time Convergence Rate of Deterministic WC-MHGD). Under Theorems 5.1 and 5.2, for any preference  $r \in \Delta_S^{++}$  and  $\epsilon > 0$ , by choosing  $\alpha \leq \frac{1}{L}$ ,  $\beta = \min\{\frac{1}{2(1+L_{\phi})r_{\max}}, \frac{1}{3L_{\phi}}\}, \ D \geq \Theta(\kappa\log\frac{1}{\epsilon}), \ N \geq \Theta(\sqrt{\kappa}\log\frac{1}{\epsilon}), \ and \ K \geq \Theta(\kappa^3\epsilon^{-1}), \ the following results of Algorithm 1 hold:$ 

• The iterates under the NS option satisfy:

$$\begin{split} &\frac{1}{K} \sum_{k=0}^{K-1} \|\bar{d}_k\|^2 \leq \frac{24 r_{\max} L_{\phi}(\phi_s(x_0) - \phi_s(x_K))}{K} \\ &+ (12 + 24 r_{\max} L_{\phi}) \cdot \left[ \left( \frac{4 M^2 (\tau \mu_g + L \rho)^2}{\mu_g^4} (1 - \alpha \mu_g)^{D-1} \right. \right. \\ &+ \left. \frac{2 L^2 (L + \mu_g)^2 (1 - \alpha \mu_g)^D}{\mu_g^2} \right) \chi + \frac{L^2 M^2 (1 - \alpha \mu_g)^{2D}}{\mu_g^2} \right], \end{split}$$

• The iterates under the CG option satisfy:

 $|v_0^*|^2$ , and  $\Gamma$  and  $\chi$  are positive constants

$$\begin{split} \frac{1}{K} \sum_{k=0}^{K-1} & \|\bar{d}_k\|^2 \leq \frac{12 r_{\max} L_{\phi} \Big( \phi_s(x_0) - \phi_s(x_K) + \delta_{D,N} \chi_0 \Big)}{K} \\ & + 24 (r_{\max} L_{\phi} + 1) M^2 \delta_{D,N} \Omega^{\frac{3}{2}} + 6 \delta_{D,N} \chi_0, \\ where & \delta_{D,N} := \Gamma (1 - \alpha \mu_g)^D + 6 L^2 \kappa \left( \frac{\sqrt{\kappa} - 1}{\sqrt{\kappa} + 1} \right)^{2N}, \Omega := \\ 4\beta^2 \left( \kappa^2 + \frac{ML}{\mu_g^2} + \frac{ML\kappa}{\mu_g^2} \right)^2, \chi_0 := \|y_0 - y^*(x_0)\|^2 + \|v_0 - y^*$$

The following oracle complexity results immediately follow from Theorem 5.5:

**Corollary 5.6** (Oracle Complexity of Deterministic WC-MHGD). To achieve an  $\epsilon$ -Pareto stationary point, by choosing D and N as Appendix D, Algorithm 1 achieves the following oracle complexities:

• NS: 
$$\operatorname{Gc}(f,\epsilon) = \mathcal{O}(\kappa^3 \epsilon^{-1} S)$$
,  $\operatorname{Gc}(g,\epsilon) = \widetilde{\mathcal{O}}(\kappa^4 \epsilon^{-1})$ ,  $\operatorname{JV}(g,\epsilon) = \widetilde{\mathcal{O}}(\kappa^4 \epsilon^{-1} S)$ ,  $\operatorname{HV}(g,\epsilon) = \widetilde{\mathcal{O}}(\kappa^4 \epsilon^{-1} S)$ .

• 
$$CG$$
:  $Gc(f, \epsilon) = \mathcal{O}(\kappa^3 \epsilon^{-1} S)$ ,  $Gc(g, \epsilon) = \widetilde{\mathcal{O}}(\kappa^4 \epsilon^{-1})$ ,  $JV(g, \epsilon) = \mathcal{O}(\kappa^3 \epsilon^{-1} S)$ ,  $HV(g, \epsilon) = \widetilde{\mathcal{O}}(\kappa^{3.5} \epsilon^{-1} S)$ .

Compared to single-objective BLO approaches (e.g., (Ji, Yang, and Liang 2021)), both options in Algorithm 1 achieve the *same* convergence rate of  $\mathcal{O}(1/K)$ . Also, all oracle complexity bounds increase by a factor of S, which is due to the fact that oracle samples are needed for each of the S UL objectives. Notably, Theorem 5.5 indicates that, even with more complex preference incorporation, our WC-MHGD approach still converges to a neighborhood of a preference-guided Pareto stationary point. This highly non-trivial preference-guided Pareto-stationarity convergence, which is similar to that of the conventional MGDA method, critically depends on our new algorithmic design in Problem (5) – a main contribution of this work as pointed out previously.

2) Convergence rate of the stochastic WC-MHGD: With the same notation as in the deterministic setting, we state the result of the stochastic WC-MHGD algorithm as follows:

**Theorem 5.7** (Finite-Time Convergence Rate of Stochastic WC-MHGD). Under Theorems 5.1 to 5.3, for any preference  $r \in \Delta_S^{++}$  and  $\epsilon > 0$ , by choosing  $\alpha = \frac{2}{L + \mu_g}$ ,  $\beta = \min\{\frac{1}{2r_{\max}(1 + L_\phi)}, \frac{1}{3L_\phi}\}$ ,  $\eta \leq \frac{1}{L}$ ,  $D = \Theta(\kappa \log(\epsilon^{-1}))$ , and  $K = \Theta(\frac{\kappa^3}{\epsilon})$ , the following results of Algorithm 2 hold:

$$\begin{split} \frac{1}{K} \sum_{k=1}^{K} \mathbb{E} \|\bar{d}_{k}\|^{2} &\leq \gamma \cdot \frac{3M^{2}(\kappa^{2}+1)}{1-\gamma} \Big(1 + 2L_{\phi}r_{max}\Big) \\ &+ \gamma \cdot \Big(6\nu + \frac{12L_{\phi}r_{max}\nu}{1-\gamma}\Big) \mathbb{E} \|y_{0} - y^{*}(x_{0})\|^{2} \\ &+ \mathcal{O}\Big(\frac{L_{\phi}}{K} + \frac{\kappa^{8}\sigma^{2}}{T} + \frac{\kappa^{5}}{D_{q}} + \frac{\kappa^{5}}{D_{f}} + \frac{\kappa^{5}}{B} + \kappa^{5}(1 - \eta\mu_{g})^{2Q}\Big), \end{split}$$

where  $\nu=\Theta(\kappa^4)$ ,  $\gamma=16\left(\frac{L-\mu_g}{L+\mu_g}\right)^{2D}\frac{\beta^2L^2\nu}{\mu_g^2}\frac{r_{\max}}{1-r_{\max}}$ ; and the batch-sizes satisfy  $|\mathcal{B}_{Q+1-j}|=BQ(1-\eta\mu_g)^{j-1}$  for  $j\in[Q]$ ,  $BQ(1-\eta\mu_g)^{Q-1}\geq 1$ ,  $Q=\Theta(\kappa\log(\kappa^2\epsilon^{-1}))$ .

The following oracle complexity results immediately follow from Theorem 5.7:

**Corollary 5.8** (Oracle Complexity of Stochastic WC-MHGD ). To achieve an  $\epsilon$ -Pareto stationary point, by choosing parameters as Appendix D, Algorithm 2 achieves the following oracle complexities:  $Gc(f,\epsilon) = \mathcal{O}(\kappa^8\epsilon^{-2}S), Gc(g,\epsilon) = \widetilde{\mathcal{O}}(\kappa^{12}\epsilon^{-2}), JV(g,\epsilon) = \mathcal{O}(\kappa^8\epsilon^{-2}S), HV(g,\epsilon) = \widetilde{\mathcal{O}}(\kappa^9\epsilon^{-2}S).$ 

Theorem 5.7 shows that, as the numbers of iterations and batch sizes increase, Algorithm 2 converges to a neighborhood of a Pareto stationary solution at rate  $\mathcal{O}(1/K)$ . Compared to the single-objective BLO approaches (e.g., (Ji, Yang, and Liang 2021)), the oracle complexity results in Theorem 5.7 increase by a factor  $\kappa^3$ . This is because stochastic MOBL methods require more data to address the bilevel error propagation issue of each UL objective and mitigate the discrepancy between approximate and true hypergradients.

Lastly, we note that preference information may not always be available in certain MOBL applications. For such MOBL problems, we can still establish their Pareto-stationarity convergence rate results in terms of  $\bar{d}_k$  under the special case without r. In fact, we show that the Pareto-stationarity convergence rate in this special case can be further tightened thanks to the simplified structure of the problem. Due to space limitations, we present this result in Appendix D.

### **6** Numerical Experiments

1) Experiment settings: 1-a) The Deterministic Setting Experiments: We use a 5-way 5-shot meta-learning task to test Algorithm 1 on the FC-100 dataset (Oreshkin, Rodríguez López, and Lacoste 2018), thus we have S=5 objectives. For these tasks, we consider multiple models comprising shared parameters and task-specific parameters. The corresponding MOBL problem involves minimizing the training loss by first determining the task-specific LL parameters and then finding the optimal shared LL parameters based on the LL solutions to minimize the validation loss. We set (K, D) = (500, 32) and u = 10 by default. We set the preference vector r as: i)  $r_s = 0.8$  for some  $s \in [S]$  and  $r_{s'} = 0.05$ ,

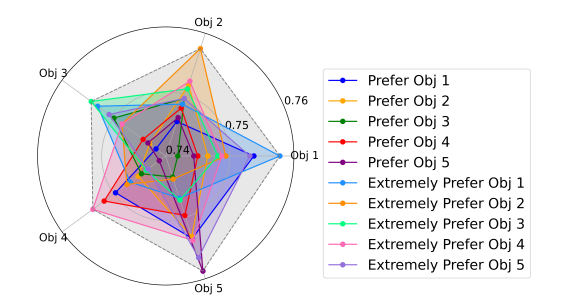


Figure 1: Pareto front exploration of Algorithm 1.

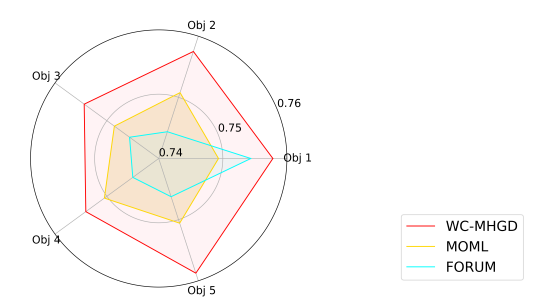


Figure 2: Comparison between algorithms.

 $\forall s' \neq s$ ; and ii)  $r_s = 0.96$  for some  $s \in [S]$  and  $r_{s'} = 0.01$ ,  $\forall s' \neq s$ . Those objectives with  $r_s = 0.8$  and  $r_s = 0.96$  are referred to as "preferred" and "extremely preferred," respectively. Each experiment is averaged over 4 trials.

1-b) The Stochastic Setting Experiments: We use a data hyper-cleaning task to test Algorithm 2 on the MNIST dataset (LeCun et al. 1998). Under 5 different corruption rates p (hence S=5 objectives), multiple models share the same UL regularization parameter based on the updates of their p-specific LL parameters. We set (K,D)=(150,200) and u=10 by default. Each experiment is averaged over 5 trials. The detailed setups can be found in Appendix E.

2) Experiment Results: Fig. 1 shows how Algorithm 1 converges to preference-guided Pareto stationary points. We can see that the accuracy of the more preferred objectives are consistently higher than those of the less preferred objectives. Moreover, for those extremely preferred objectives, this trend becomes more pronounced. The outer gray area demonstrates that our WC-MHGD algorithm effectively explores a large Pareto stationarity footprint. Fig. 2 highlights that Pareto exploration allows Algorithm 1 to cover a larger portion of Pareto front, compared to MOML (Ye et al. 2021) and FORUM (Ye et al. 2024). Due to space limitation, we relegate further experimental details and results in Appendix E.

#### 7 Conclusion

In this paper, we investigated MOBL problems and proposed a unifying WC-MHGD algorithmic framework, which offers finite-time Pareto-stationarity convergence guarantees, low oracle complexities, and systematic Pareto-stationarity front exploration capability. Our numerical results further verified the effectiveness of our proposed algorithms.

## Acknowledgement

This work is supported in part by Meta Research Award INB3267726, NSF grants CAREER CNS-2110259, CNS-2112471, and ECCS-233104, DARPA grants YFA D24AP00265 and HR0011-25-2-0019, and ONR grant N00014-24-1-2729.

### References

- Abdi, A.; and Kaveh, M. 2002. A space-time correlation model for multielement antenna systems in mobile fading channels. *IEEE Journal on Selected Areas in communications*, 20(3): 550–560.
- AL-Gburi, A. F. J.; Nazri, M. Z. A.; Yaakub, M. R. B.; and Alyasseri, Z. A. A. 2024. Multi-objective unsupervised feature selection and cluster based on symbiotic organism search. *Algorithms*, 17(8): 355.
- Alok, A. K.; Saha, S.; and Ekbal, A. 2015. A new semisupervised clustering technique using multi-objective optimization. *Applied Intelligence*, 43: 633–661.
- Arbel, M.; and Mairal, J. 2021. Amortized implicit differentiation for stochastic bilevel optimization. *arXiv* preprint *arXiv*:2111.14580.
- Arjovsky, M.; Bottou, L.; Gulrajani, I.; and Lopez-Paz, D. 2019. Invariant risk minimization. *arXiv preprint arXiv:1907.02893*.
- Arnold, S. M.; Mahajan, P.; Datta, D.; Bunner, I.; and Zarkias, K. S. 2020. learn2learn: A library for meta-learning research. *arXiv preprint arXiv:2008.12284*.
- Aşkan, A.; and Sayın, S. 2014. SVM classification for imbalanced data sets using a multiobjective optimization framework. *Annals of Operations Research*, 216: 191–203.
- Borsos, Z.; Mutny, M.; and Krause, A. 2020. Coresets via bilevel optimization for continual learning and streaming. *Advances in neural information processing systems*, 33: 14879–14890.
- Bracken, J.; and McGill, J. T. 1973. Mathematical programs with optimization problems in the constraints. *Operations Research*, 21(1): 37–44.
- Chakraborty, S.; Bedi, A.; Koppel, A.; Wang, H.; Manocha, D.; Wang, M.; and Huang, F. 2024. Parl: A unified framework for policy alignment in reinforcement learning from human feedback. In *The Twelfth International Conference on Learning Representations*.
- Chankong, V.; and Haimes, Y. Y. 2008. *Multiobjective decision making: theory and methodology*. Courier Dover Publications.
- Chen, L.; Saif, A.; Shen, Y.; and Chen, T. 2024. FERERO: A Flexible Framework for Preference-Guided Multi-Objective Learning. *arXiv* preprint arXiv:2412.01773.
- Chen, T.; Sun, Y.; Xiao, Q.; and Yin, W. 2022. A single-timescale method for stochastic bilevel optimization. In *International Conference on Artificial Intelligence and Statistics*, 2466–2488. PMLR.
- Chen, Y.; Li, Z.; Yang, B.; Nai, K.; and Li, K. 2020. A Stackelberg game approach to multiple resources allocation

- and pricing in mobile edge computing. *Future Generation Computer Systems*, 108: 273–287.
- Coello, C. A. C. 2007. Evolutionary algorithms for solving multi-objective problems. Springer.
- Colson, B.; Marcotte, P.; and Savard, G. 2007. An overview of bilevel optimization. *Annals of operations research*, 153(1): 235–256.
- Crawshaw, M. 2020. Multi-task learning with deep neural networks: A survey. *arXiv preprint arXiv:2009.09796*.
- Crockett, C.; Fessler, J. A.; et al. 2022. Bilevel methods for image reconstruction. *Foundations and Trends® in Signal Processing*, 15(2-3): 121–289.
- Dagréou, M.; Ablin, P.; Vaiter, S.; and Moreau, T. 2022. A framework for bilevel optimization that enables stochastic and global variance reduction algorithms. *Advances in Neural Information Processing Systems*, 35: 26698–26710.
- Désidéri, J.-A. 2012. Multiple-gradient descent algorithm (MGDA) for multiobjective optimization. *Comptes Rendus Mathematique*, 350(5-6): 313–318.
- Elsken, T.; Metzen, J. H.; and Hutter, F. 2018. Efficient multiobjective neural architecture search via lamarckian evolution. arXiv preprint arXiv:1804.09081.
- Fernando, H.; Shen, H.; Liu, M.; Chaudhury, S.; Murugesan, K.; and Chen, T. 2022. Mitigating gradient bias in multi-objective learning: A provably convergent stochastic approach. *arXiv preprint arXiv:2210.12624*.
- Finn, C.; Abbeel, P.; and Levine, S. 2017. Model-agnostic meta-learning for fast adaptation of deep networks. In *International conference on machine learning*, 1126–1135. PMLR.
- Franceschi, L.; Frasconi, P.; Salzo, S.; Grazzi, R.; and Pontil, M. 2018. Bilevel programming for hyperparameter optimization and meta-learning. In *International conference on machine learning*, 1568–1577. PMLR.
- Ghadimi, S.; and Wang, M. 2018. Approximation methods for bilevel programming. *arXiv preprint arXiv:1802.02246*.
- Golovin, D.; and Zhang, Q. 2020. Random Hypervolume Scalarizations for Provable Multi-Objective Black Box Optimization. *ArXiv*, abs/2006.04655.
- Gong, M.; Zhang, M.; and Yuan, Y. 2015. Unsupervised band selection based on evolutionary multiobjective optimization for hyperspectral images. *IEEE Transactions on Geoscience and Remote Sensing*, 54(1): 544–557.
- Gong, X.; Hao, J.; and Liu, M. 2024. An accelerated algorithm for stochastic bilevel optimization under unbounded smoothness. *arXiv preprint arXiv:2409.19212*.
- González-Almagro, G.; Rosales-Pérez, A.; Luengo, J.; Cano, J.-R.; and García, S. 2020. Improving constrained clustering via decomposition-based multiobjective optimization with memetic elitism. In *Proceedings of the 2020 Genetic and Evolutionary Computation Conference*, 333–341.
- Gu, A.; Lu, S.; Ram, P.; and Weng, T.-W. 2023. Min-max multi-objective bilevel optimization with applications in robust machine learning. In *The Eleventh International Conference on Learning Representations*.

- Gunantara, N. 2018. A review of multi-objective optimization: Methods and its applications. *Cogent Engineering*, 5(1): 1502242.
- Hong, M.; Wai, H.-T.; Wang, Z.; and Yang, Z. 2023. A two-timescale stochastic algorithm framework for bilevel optimization: Complexity analysis and application to actorcritic. *SIAM Journal on Optimization*, 33(1): 147–180.
- Hospedales, T.; Antoniou, A.; Micaelli, P.; and Storkey, A. 2021. Meta-learning in neural networks: A survey. *IEEE transactions on pattern analysis and machine intelligence*, 44(9): 5149–5169.
- Hu, Y.; Wang, J.; Xie, Y.; Krause, A.; and Kuhn, D. 2023. Contextual stochastic bilevel optimization. *Advances in Neural Information Processing Systems*, 36: 78412–78434.
- Hwang, C.-L.; and Masud, A. S. M. 2012. *Multiple objective decision making—methods and applications: a state-of-the-art survey*, volume 164. Springer Science & Business Media.
- Ji, K.; Yang, J.; and Liang, Y. 2021. Bilevel optimization: Convergence analysis and enhanced design. In *International conference on machine learning*, 4882–4892. PMLR.
- Jin, Y.; Wen, R.; and Sendhoff, B. 2007. Evolutionary multiobjective optimization of spiking neural networks. In *International Conference on Artificial Neural Networks*, 370–379. Springer.
- Karl, F.; Pielok, T.; Moosbauer, J.; Pfisterer, F.; Coors, S.; Binder, M.; Schneider, L.; Thomas, J.; Richter, J.; Lang, M.; et al. 2023. Multi-objective hyperparameter optimization in machine learning—An overview. *ACM Transactions on Evolutionary Learning and Optimization*, 3(4): 1–50.
- Khanduri, P.; Zeng, S.; Hong, M.; Wai, H.-T.; Wang, Z.; and Yang, Z. 2021. A near-optimal algorithm for stochastic bilevel optimization via double-momentum. *Advances in neural information processing systems*, 34: 30271–30283.
- Konak, A.; Coit, D. W.; and Smith, A. E. 2006. Multiobjective optimization using genetic algorithms: A tutorial. *Reliability engineering & system safety*, 91(9): 992–1007.
- Krizhevsky, A.; Hinton, G.; et al. 2009. Learning multiple layers of features from tiny images.(2009).
- Kunapuli, G.; Bennett, K. P.; Hu, J.; and Pang, J.-S. 2008. Classification model selection via bilevel programming. *Optimization Methods & Software*, 23(4): 475–489.
- Kwon, J.; Kwon, D.; Wright, S.; and Nowak, R. D. 2023. A fully first-order method for stochastic bilevel optimization. In *International Conference on Machine Learning*, 18083–18113. PMLR.
- LeCun, Y.; Bottou, L.; Bengio, Y.; and Haffner, P. 1998. Gradient-based learning applied to document recognition. *Proceedings of the IEEE*, 86(11): 2278–2324.
- Li, F.; Yang, Y.; Liu, Y.; Liu, Y.; and Qian, M. 2024. Bi-Level Model Management Strategy for Solving Expensive Multi-Objective Optimization Problems. *IEEE Transactions* on Emerging Topics in Computational Intelligence.
- Lin, S.; Sow, D.; Ji, K.; Liang, Y.; and Shroff, N. 2024a. Non-convex bilevel optimization with time-varying objective functions. *Advances in Neural Information Processing Systems*, 36.

- Lin, X.; Zhang, X.; Yang, Z.; Liu, F.; Wang, Z.; and Zhang, Q. 2024b. Smooth Tchebycheff Scalarization for Multi-Objective Optimization. *arXiv* preprint arXiv:2402.19078.
- Lin, X.; Zhen, H.-L.; Li, Z.; Zhang, Q.-F.; and Kwong, S. 2019. Pareto multi-task learning. *Advances in neural information processing systems*, 32.
- Liu, H.; Simonyan, K.; and Yang, Y. 2018. Darts: Differentiable architecture search. *arXiv preprint arXiv:1806.09055*.
- Liu, R.; Liu, Y.; Yao, W.; Zeng, S.; and Zhang, J. 2023a. Averaged method of multipliers for bi-level optimization without lower-level strong convexity. In *International Conference on Machine Learning*, 21839–21866. PMLR.
- Liu, R.; Mu, P.; Yuan, X.; Zeng, S.; and Zhang, J. 2020. A generic first-order algorithmic framework for bi-level programming beyond lower-level singleton. In *International conference on machine learning*, 6305–6315. PMLR.
- Liu, Z.; Zhang, X.; Khanduri, P.; Lu, S.; and Liu, J. 2023b. Prometheus: taming sample and communication complexities in constrained decentralized stochastic bilevel learning. In *International Conference on Machine Learning*, 22420–22453. PMLR.
- Lobato, F.; Sales, C.; Araujo, I.; Tadaiesky, V.; Dias, L.; Ramos, L.; and Santana, A. 2015. Multi-objective genetic algorithm for missing data imputation. *Pattern Recognition Letters*, 68: 126–131.
- Mahapatra, D.; and Rajan, V. 2020. Multi-task learning with user preferences: Gradient descent with controlled ascent in pareto optimization. In *International Conference on Machine Learning*, 6597–6607. PMLR.
- Mehra, A.; and Hamm, J. 2021. Penalty method for inversion-free deep bilevel optimization. In *Asian Conference on Machine Learning*, 347–362. PMLR.
- Mercier, Q.; Poirion, F.; and Désidéri, J.-A. 2018. A stochastic multiple gradient descent algorithm. *European Journal of Operational Research*, 271(3): 808–817.
- Miettinen, K.; and Mäkelä, M. 1995. Interactive bundle-based method for nondifferentiable multiobjeective optimization: Nimbus. *Optimization*, 34(3): 231–246.
- Momma, M.; Dong, C.; and Liu, J. 2022. A multi-objective/multi-task learning framework induced by pareto stationarity. In *International Conference on Machine Learning*, 15895–15907. PMLR.
- Mossalam, H.; Assael, Y. M.; Roijers, D. M.; and Whiteson, S. 2016. Multi-objective deep reinforcement learning. *arXiv* preprint arXiv:1610.02707.
- Oreshkin, B.; Rodríguez López, P.; and Lacoste, A. 2018. Tadam: Task dependent adaptive metric for improved fewshot learning. *Advances in neural information processing systems*, 31.
- Peitz, S.; and Hotegni, S. S. 2024. Multi-objective Deep Learning: Taxonomy and Survey of the State of the Art. *arXiv* preprint *arXiv*:2412.01566.
- Qiu, P.; Li, Y.; Liu, Z.; Khanduri, P.; Liu, J.; Shroff, N. B.; Bentley, E. S.; and Turck, K. 2023. DIAMOND: Taming Sample and Communication Complexities in Decentralized

- Bilevel Optimization. In *IEEE INFOCOM 2023-IEEE Conference on Computer Communications*, 1–10. IEEE.
- Qiu, S.; Zhang, D.; Yang, R.; Lyu, B.; and Zhang, T. 2024. Traversing Pareto Optimal Policies: Provably Efficient Multi-Objective Reinforcement Learning. arXiv:2407.17466.
- Sawaragi, Y.; NAKAYAMA, H.; and TANINO, T. 1985. *Theory of multiobjective optimization*. Elsevier.
- Sener, O.; and Koltun, V. 2018. Multi-task learning as multiobjective optimization. *Advances in neural information processing systems*, 31.
- Shaban, A.; Cheng, C.-A.; Hatch, N.; and Boots, B. 2019. Truncated back-propagation for bilevel optimization. In *The 22nd International Conference on Artificial Intelligence and Statistics*, 1723–1732. PMLR.
- Shen, H.; Yang, Z.; and Chen, T. 2024. Principled penalty-based methods for bilevel reinforcement learning and rlhf. *arXiv preprint arXiv:2402.06886*.
- Shi, C.; Lu, J.; and Zhang, G. 2005. An extended Kuhn–Tucker approach for linear bilevel programming. *Applied Mathematics and Computation*, 162(1): 51–63.
- Sow, D.; Ji, K.; and Liang, Y. 2022. On the convergence theory for hessian-free bilevel algorithms. *Advances in Neural Information Processing Systems*, 35: 4136–4149.
- Sun, H.; Chen, X.; Shi, Q.; Hong, M.; Fu, X.; and Sidiropoulos, N. D. 2018. Learning to optimize: Training deep neural networks for interference management. *IEEE Transactions on Signal Processing*, 66(20): 5438–5453.
- Wang, B.; Singh, H. K.; and Ray, T. 2024. Pareto Set Prediction Assisted Bilevel Multi-objective Optimization. *arXiv* preprint arXiv:2409.03328.
- Xiao, P.; and Ji, K. 2023. Communication-efficient federated hypergradient computation via aggregated iterative differentiation. In *International Conference on Machine Learning*, 38059–38086. PMLR.
- Xu, M.; Ju, P.; Liu, J.; and Yang, H. 2024. PSMGD: Periodic Stochastic Multi-Gradient Descent for Fast Multi-Objective Optimization. *arXiv* preprint arXiv:2412.10961.
- Yang, H.; Liu, Z.; Liu, J.; Dong, C.; and Momma, M. 2024a. Federated multi-objective learning. *Advances in Neural Information Processing Systems*, 36.
- Yang, J.; Ji, K.; and Liang, Y. 2021. Provably faster algorithms for bilevel optimization. *Advances in Neural Information Processing Systems*, 34: 13670–13682.
- Yang, P.; Lao, Y.; and Li, P. 2021. Robust watermarking for deep neural networks via bi-level optimization. In *Proceedings of the IEEE/CVF international conference on computer vision*, 14841–14850.
- Yang, X.; Yao, W.; Yin, H.; Zeng, S.; and Zhang, J. 2024b. Gradient-based algorithms for multi-objective bi-level optimization. *Science China Mathematics*, 1–20.
- Yang, Y.; Xiao, P.; and Ji, K. 2023. Achieving  $O(\epsilon^{-1.5})$  Complexity in Hessian/Jacobian-free Stochastic Bilevel Optimization. arXiv:2312.03807.
- Ye, F.; Lin, B.; Cao, X.; Zhang, Y.; and Tsang, I. W. 2024. A first-order multi-gradient algorithm for multi-objective bilevel optimization. In *ECAI 2024*, 2621–2628. IOS Press.

- Ye, F.; Lin, B.; Yue, Z.; Guo, P.; Xiao, Q.; and Zhang, Y. 2021. Multi-objective meta learning. *Advances in Neural Information Processing Systems*, 34: 21338–21351.
- Zhang, Y.; Khanduri, P.; Tsaknakis, I.; Yao, Y.; Hong, M.; and Liu, S. 2024. An Introduction to Bilevel Optimization: Foundations and applications in signal processing and machine learning. *IEEE Signal Processing Magazine*, 41(1): 38–59.
- Zhang, Y.; Yao, Y.; Ram, P.; Zhao, P.; Chen, T.; Hong, M.; Wang, Y.; and Liu, S. 2022. Advancing model pruning via bi-level optimization. *Advances in Neural Information Processing Systems*, 35: 18309–18326.
- Zhou, T.; Hairi, F.; Yang, H.; Liu, J.; Tong, T.; Yang, F.; Momma, M.; and Gao, Y. 2024. Finite-time convergence and sample complexity of actor-critic multi-objective reinforcement learning. *arXiv* preprint arXiv:2405.03082.
- Zuo, S.; Liang, C.; Jiang, H.; Liu, X.; He, P.; Gao, J.; Chen, W.; and Zhao, T. 2021. Adversarial regularization as stackelberg game: An unrolled optimization approach. *arXiv* preprint arXiv:2104.04886.

### **A** Notations

We summarize the notations throughout this paper in Table 1.

Notations	Definitions
$d_k$ with preferences	$d_k = \hat{\nabla}\Phi(x_k)(r \odot \lambda_k)$
$\bar{d}_k$ with preferences	$\bar{d}_k = \nabla \Phi(x_k)(r \odot \lambda_k)$
$d_k$ without preferences	$d_k = \hat{\nabla}\Phi(x_k)\lambda_k = \sum_{s=1}^S \lambda_k^{(s)} \hat{\nabla}\phi_s(x_k)$ $\bar{d}_k = \nabla\Phi(x_k)\lambda_k = \sum_{s=1}^S \lambda_k^{(s)} \nabla\phi_s(x_k)$
$ar{d}_k$ without preferences	$\bar{d}_k = \nabla \Phi(x_k) \lambda_k = \sum_{s=1}^S \lambda_k^{(s)} \nabla \phi_s(x_k)$
$[S] \parallel \cdot \parallel$	Set of integers $\{1,\ldots,S\}$
	$l_2$ -norm
$\hat{\nabla}\Phi(x) \in \mathbb{R}^{p \times S}$	$\hat{\nabla}\Phi(x)$ is a p by S matrix
$r \in \mathbb{R}^{S}_{++}$ $\Delta^{+}_{S}$ $\Delta^{+}_{S}$	$r$ is a strictly positive vector in $\mathbb{R}^S$
$\Delta_S^+$	Simplex in $S$ dimension
$\Delta_S^{\mp+}$	Strictly positive simplex in $S$ dimension
$e_s$	A vector with 1 in the $s$ -th position and 0 otherwise
1	A vector with 1 as all elements
$\odot$	Hadamard product notation

Table 1: Summarized notation table in the paper.

# B Related work and comparison between WC-MHGD and existing algorithms

In this section, we provide an overview on two closely related research areas, namely MOO, BLO, and the comparison between our WC-MHGD approach and recent works in MOBL.

- 1) Multi-objective Optimization (MOO): The research on MOO dates back to (Sawaragi, NAKAYAMA, and TANINO 1985) and has been actively studied to this date (see, e.g., (Chankong and Haimes 2008; Hwang and Masud 2012; Gunantara 2018) for overviews). In recent years, thanks to the rise of ML problems with first-order oracles being readily accessible, gradient-based MOO approaches have gained increasing attention. Numerous gradient-based MOO algorithms have been proposed (Désidéri 2012; Mercier, Poirion, and Désidéri 2018; Miettinen and Mäkelä 1995; Coello 2007; Elsken, Metzen, and Hutter 2018; Xu et al. 2024; Momma, Dong, and Liu 2022; Mahapatra and Rajan 2020; Lin et al. 2024b; Chen et al. 2024), with applications spanning multi-task learning (Sener and Koltun 2018; Momma, Dong, and Liu 2022; Crawshaw 2020; Lin et al. 2019), feature selection (Peitz and Hotegni 2024; AL-Gburi et al. 2024; Gong, Zhang, and Yuan 2015), multi-objective training and clustering (Mossalam et al. 2016; Aşkan and Sayın 2014; Alok, Saha, and Ekbal 2015; González-Almagro et al. 2020), architecture search (Jin, Wen, and Sendhoff 2007), hyper-parameter optimization (Karl et al. 2023), data imputation (Lobato et al. 2015), to name a few. However, none of these gradient-based MOO approaches considered bilevel-type problem structure. In contrast, our work proposes the first set of multi-objective bilevel algorithms designed to achieve Pareto-stationary solutions and explore Pareto front guided by preferences, with theoretical finite-time convergence guarantees.
- 2) Bilevel Optimization (BLO): Similar to MOO, BLO also has a long research and, to our knowledge, the earliest work on BLO appeared in (Bracken and McGill 1973). Over the years, several BLO approaches have been proposed, including 1) penalizing the UL function with the optimality conditions of the LL problem (Shi, Lu, and Zhang 2005; Mehra and Hamm 2021); 2) reformulating the BLO problem as a single-level problem by replacing the LL problem with its optimality conditions (Colson, Marcotte, and Savard 2007; Kunapuli et al. 2008); and 3) utilizing hypergradient-based techniques to iteratively approximate the (stochastic) gradient of the UL problem. In the ML literature, hypergradient-based BLO approaches have gained the most attention in recent years also thanks to their exploitation of first-order oracles in ML models. To date, numerous hypergradient-based bilevel optimization algorithms have been proposed, including but not limited to (Ghadimi and Wang 2018; Ji, Yang, and Liang 2021; Yang, Ji, and Liang 2021; Sow, Ji, and Liang 2022; Yang, Xiao, and Ji 2023; Arbel and Mairal 2021; Kwon et al. 2023; Dagréou et al. 2022; Hong et al. 2023; Khanduri et al. 2021), with applications in signal processing (Abdi and Kaveh 2002; Crockett, Fessler et al. 2022; Chen et al. 2020; Sun et al. 2018), adversarial training (Zuo et al. 2021; Yang, Lao, and Li 2021), model-agnostic meta-learning (Finn, Abbeel, and Levine 2017; Arjovsky et al. 2019), efficient machine learning (Borsos, Mutny, and Krause 2020; Zhang et al. 2022), and model pruning (Liu et al. 2020; Liu, Simonyan, and Yang 2018). However, these existing hypergradient-based approaches are all designed for single UL objective setting. In this work, we generalize hypergradient BLO algorithms to the MOO settings.
- 3) **Detailed comparison:** We summarize the comparison between our WC-MHGD approach and some existing BLO and MOBL algorithms in Table 2 as follows.

Algorithm	Problem	Scenario	Finite-time	Rate	Preference
AID(Ji, Yang, and Liang 2021)	BLO	Deterministic	Yes	$\mathcal{O}(K^{-1})$	-
ITD(Ji, Yang, and Liang 2021)	BLO	Deterministic	Yes	$\mathcal{O}(K^{-1})$	-
SOBA(Dagréou et al. 2022)	BLO	Stochastic	Yes	$\mathcal{O}(K^{-rac{1}{2}})$	-
STABLE(Chen et al. 2022)	BLO	Stochastic	Yes	$\mathcal{O}(K^{-\frac{1}{2}})$	-
stocBiO(Ji, Yang, and Liang 2021)	BLO	Stochastic	Yes	$\mathcal{O}(K^{-1})$	-
AmIGO(Arbel and Mairal 2021)	BLO	Stochastic	Yes	$\mathcal{O}(K^{-1})$	-
BLMS(Li et al. 2024)	MOBL	Deterministic	No	-	No
PSP-BLEMO(Wang, Singh, and Ray 2024)	MOBL	Deterministic	No	-	No
MOML(Ye et al. 2021)	MOBL	Deterministic	No	-	No
gMOBA(Yang et al. 2024b)	MOBL	Deterministic	No	-	No
FORUM(Ye et al. 2024)	MOBL	Deterministic	Yes	$\mathcal{O}(K^{-\frac{1}{4}})$	No
MoCo(Fernando et al. 2022)	MOBL	Stochastic	Yes	$\mathcal{O}(SK^{-\frac{1}{2}})$	No
WC-MHGD (ours)	MOBL	Deterministic	Yes	$\mathcal{O}(K^{-1})$	Yes
WC-MHGD (ours)	MOBL	Stochastic	Yes	$\mathcal{O}(K^{-1})$	Yes

Table 2: Comparison between WC-MHGD and existing BLO and MOBL algorithms. *Problem* indicates whether the work considers BLO or MOBL problem, *Scenario* specifies whether the setting is deterministic or stochastic, *Finite-time* means whether the work provides a finite-time convergence guarantee or not, *Rate* means the theoretical finite-time convergence rate (if exists), and *Preference* means whether the work take user preference into account.

# C Geometric interpretation of WC-MHGD design

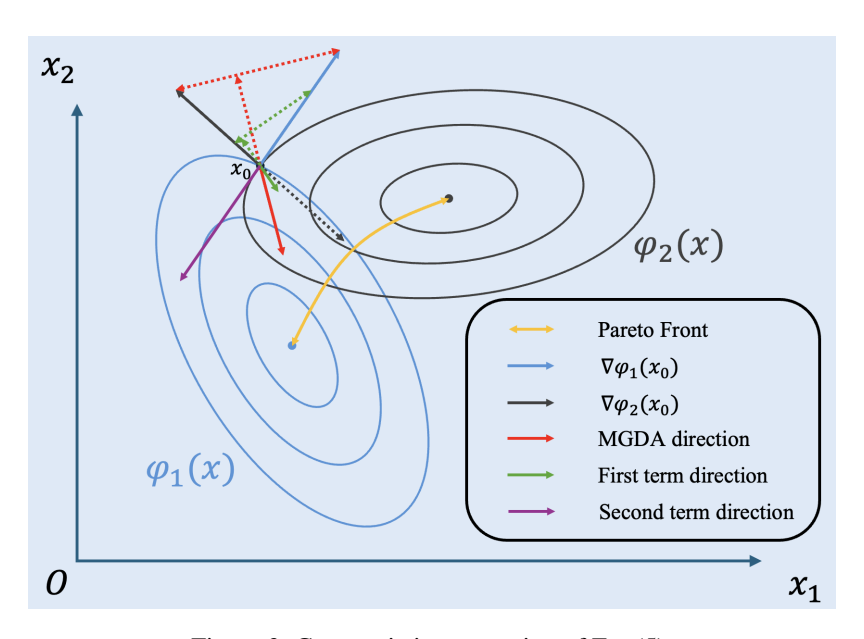


Figure 3: Geometric interpretation of Eq. (5).

To better understand Eq. (5), we provide a geometric interpretation of illustrated in Fig. 3. Consider a scenario with two objectives, represented by the blue and dark gray contours, respectively. Suppose  $\phi_1(x)$  is more preferred, implying  $r_1 > r_2$ . We also assume that two objectives are of comparable scaling. We can observe the following facts: (1) At current  $x_0$ , MGDA (red arrow) minimizes  $\|\lambda \cdot \nabla \phi_1(x_0) + (1-\lambda) \cdot \nabla \phi_2(x_0)\|^2$  to approach Pareto front, meaning it finds a point x' on the line segment formed by the endpoints of  $\nabla \phi_1(x_0)$  and  $\nabla \phi_2(x_0)$  to minimize the length of  $x' - x_0$ . (2) Minimizing the first term of Equation (5) corresponds to finding a point x'' on the green dashed line segment to minimize the length of  $x'' - x_0$ , i.e., to minimize  $\|\lambda \cdot r_1 \nabla \phi_1(x_0) + (1-\lambda) \cdot r_2 \nabla \phi_2(x_0))\|^2$ . As a result, the generated direction (green arrow) also converges to Pareto front. (3) As for the second term, minimizing it is equivalent to maximizing  $\lambda \cdot r_1 \phi_1(x_0) + (1-\lambda) \cdot r_2 \phi_2(x_0)$ . Since two objectives share a similar scale, the preference implies  $r_1 \phi_1(x_0) > r_2 \phi_2(x_0)$ . Therefore, the maximization naturally leads to selecting  $\lambda = 1$  since  $\lambda \in \Delta_2^+$ . This emphasizes the purple arrow in Figure 3, which is known as the steepest descent direction for  $\phi_1(x_0)$ .

Remark 1. As mentioned earlier, the primal WC problem aims to minimize the weighted loss in  $l_{\infty}$ -norm sense by minimizing  $\gamma$ , such that  $r\odot\Phi(x)\leq\gamma$ 1. We argue that the second term in Equation (5) aligns with this idea. This term consistently points toward the steepest descent direction of the objective s with maximal  $r_s\phi_s(x)$ , depicted as the purple arrow in Figure 3. Therefore, it effectively control the dominant term in  $r\odot\Phi(x)$ , thus continuously reduces its  $l_{\infty}$ -norm.

Remark 2. Another remark is that the positive constant u in Equation (5) plays a role as a trade-off controller. Since  $d_k$  is a combination of the green and purple arrows in Figure 3, it's obvious that a larger u yields a solution more closely aligned with the preference; while a smaller u ensures a tighter adherence to the stationarity condition.

*Remark 3.* It is also worth noting that, for simplicity in this geometric interpretation, we replace hyper-gradients with true gradients. This simplification highlights that since inaccuracies caused by bilevel structures can lead to deviations in the descent direction, such deviations necessitate careful algorithm design to mitigate their impact.

### **D** Theoretical proofs

In this section, we begin by proving two key lemmas presented in Section 4 and Section 5. Next, we provide a detailed analysis of the two main theoretical results: Theorem 5.5 and Theorem 5.7. Finally, we present an additional finding: if the MOBL problem is not provided by any user preference vector r, which is exactly the fourth type of philosophy mentioned in Section 3, then this scenario can be treated as a special case of our WC-MHGD framework.

#### D.1 Proof of Theorem 4.3

*Proof.* We first give the Pareto stationarity condition: If  $\lambda$  satisfies the following conditions:

$$K\lambda = 0, \mathbf{1}^{\top}\lambda = 1, \lambda \ge 0, \tag{6}$$

then it provides Pareto stationarity (Désidéri 2012; Sener and Koltun 2018; Momma, Dong, and Liu 2022). According to our assumptions,  $\lambda$ , on the other hand, satisfies the following conditions:

$$K(r \odot \lambda) = K \operatorname{diag}(r)\lambda = 0, \mathbf{1}^{\top} \lambda = 1, \lambda \ge 0.$$
 (7)

We denote  $\operatorname{diag}(r)\lambda = \tilde{\lambda}$ , which implies  $K\tilde{\lambda} = 0$  and  $\tilde{\lambda} \geq 0$ . Since  $\lambda \geq 0$  and  $\mathbf{1}^{\top}\lambda = 1$ , there must exist at least one positive element  $\lambda_i$  in  $\lambda$ . Moreover, since r is strictly positive, we can further attain  $\tilde{\lambda}_i > 0$ . Now, we rescale as follows:

$$\hat{\lambda} = \frac{\tilde{\lambda}}{\mathbf{1}^{\top} \tilde{\lambda}},\tag{8}$$

which is valid since  $\mathbf{1}^{\top}\tilde{\lambda} \geq \tilde{\lambda}_i > 0$ . Therefore, we check Pareto stationarity condition Equation (6) on  $\hat{\lambda}$  to end the proof:

$$K\hat{\lambda} = 0, \mathbf{1}^{\top}\hat{\lambda} = 1, \hat{\lambda} \ge 0. \tag{9}$$

*Remark.* It is obvious that during the iterations prior to convergence, satisfying  $K(r \odot \lambda) = 0$  is almost impossible to be satisfied. To this end, we minimize  $||K(r \odot \lambda)||^2$  to yield stationarity in Equation (5), which serves as a reasonable and practical surrogate of  $K(r \odot \lambda) = 0$  for achieving Pareto stationarity.

#### D.2 Proof of Theorem 5.4

*Proof.* For any feasible  $\lambda$ , we denote its corresponding direction as  $d = \hat{\nabla}\Phi(x_k)(r \odot \lambda)$ . Let  $d = d_k + v$ . It is obvious that Equation (5) is a convex optimization problem. Therefore, for any  $\epsilon \in [0,1]$ , we know that the weight vector of  $d_k + \epsilon v$  is also feasible, and its corresponding weight vector  $\lambda(\epsilon) = \lambda_k + \epsilon(\lambda - \lambda_k)$ , since:

$$\begin{split} d_k + \epsilon v &= d_k + \epsilon (d - d_k) \\ &= (1 - \epsilon) d_k + \epsilon d \\ &= (1 - \epsilon) \hat{\nabla} \Phi(x_k) (r \odot \lambda_k) + \epsilon \hat{\nabla} \Phi(x_k) (r \odot \lambda) \\ &= (1 - \epsilon) \hat{\nabla} \Phi(x_k) \mathrm{diag}(r) \lambda_k + \epsilon \hat{\nabla} \Phi(x_k) \mathrm{diag}(r) \lambda \\ &= \hat{\nabla} \Phi(x_k) \mathrm{diag}(r) \left[ \lambda_k + \epsilon (\lambda - \lambda_k) \right]. \end{split}$$

Since  $\lambda_k$  is the optima of Equation (5), we have:

$$||K(r \odot \lambda_k)||^2 - u\lambda_k^\top (r \odot \Phi(x_k)) \le ||K(r \odot \lambda(\epsilon))||^2 - u\lambda(\epsilon)^\top (r \odot \Phi(x_k)),$$

which, since  $||K\lambda||^2 = ||\hat{\nabla}\Phi(x_k)\lambda||^2$ , is equivalent to:

$$||d_k||^2 - u\lambda_k^\top (r \odot \Phi(x_k)) \le ||d_k + \epsilon v||^2 - u(\lambda_k + \epsilon(\lambda - \lambda_k))^\top (r \odot \Phi(x_k)).$$

Thus, after decomposing the first term in RHS and rearranging the inequality, we obtain:

$$2\epsilon \langle d_k, v \rangle + \epsilon^2 ||v||^2 \ge \epsilon u(\lambda - \lambda_k)^\top (r \odot \Phi(x_k)).$$

From last inequality, we can observe that  $(\lambda - \lambda_k)$  is bounded, thus, we can select a small enough u, such that  $u(\lambda - \lambda_k)^{\top}(r \odot \Phi(x_k)) \leq \|d_k\|^2$ . Simultaneously, we let  $\epsilon$  go to 0 to get:

$$2\langle d_k, d \rangle \ge ||d_k||^2. \tag{10}$$

Now, we note that for any  $s \in [S]$ , we have  $\hat{\nabla}\phi_s(x_k) = \hat{\nabla}\Phi(x_k)e_s$ , where  $e_s$  is the vector with element 1 in the s-th position and 0 in all other positions. It is trivial that  $e_s$  is feasible for Equation (5) for any  $s \in [S]$ . Let  $r_s$  be the s-th element of preference r, then we find the corresponding direction of  $e_s$  has the following form:

$$\hat{\nabla}\Phi(x_k)(r\odot e_s) = \hat{\nabla}\Phi(x_k)\operatorname{diag}(r)e_s = r_s\hat{\nabla}\phi_s(x_k).$$

Substituting this result into Equation (10), we have:

$$||d_k||^2 \le 2r_s \langle d_k, \hat{\nabla} \phi_s(x_k) \rangle.$$

Therefore, for any  $s \in [S]$ , we have:  $||d_k||^2 \le 2r_{\max} \langle d_k, \hat{\nabla} \phi_s(x_k) \rangle$ .

#### D.3 Proof of Theorem 5.5

We prove Theorem 5.5 in this section. To make it more clear, we prove Theorem 5.5 under option NS and option CG separately.

*Proof.* (**Theorem 5.5 under option NS**) We first give the following lemma, inspired by (Ji, Yang, and Liang 2021), which quantifies the gap of true gradients and hyper-gradients when leveraging NS approximation. In other words, it ensures the error caused by bilevel structure can be well controlled, thus won't lead to more inaccuracy.

**Lemma D.1.** When using Algorithm 1 with NS to compute  $\hat{\nabla}\phi_s(x_k)$  with  $\alpha \leq \frac{1}{L}$ , we have the following result for each  $s \in \mathcal{S}$  and  $k \in \{0, 1, \dots, K-1\}$ :

$$\|\nabla\phi_{s}(x_{k}) - \hat{\nabla}\phi_{s}(x_{k})\|$$

$$\leq \left(\frac{L(L + \mu_{g})(1 - \alpha\mu_{g})^{\frac{D}{2}}}{\mu_{g}} + \frac{2M(\tau\mu_{g} + L\rho)}{\mu_{g}^{2}}(1 - \alpha\mu_{g})^{\frac{D-1}{2}}\right)\|y_{k}^{0} - y^{*}(x_{k})\|$$

$$+ \frac{LM(1 - \alpha\mu_{g})^{D}}{\mu_{g}}.$$

From the Theorem 5.2, we attain that the upper level function  $\phi_s(x)$  is also smooth for every  $s \in \mathcal{S}$ , and we denote the positive Lipschitz constant as  $L_{\phi} = L + \frac{2L^2 + \tau M^2}{\mu_g} + \frac{\rho L M + L^3 + \tau L M}{\mu_g^2} + \frac{\rho L^2 M}{\mu_g^3} = \Theta(\kappa^3)$ . Thus, we have the following descent lemma for each  $s \in \mathcal{S}$ :

$$\phi_s(x_{k+1}) \le \phi_s(x_k) + \langle \nabla \phi_s(x_k), x_{k+1} - x_k \rangle + \frac{L_\phi}{2} \|x_{k+1} - x_k\|^2, \tag{11}$$

where  $k \in \{0, 1, \dots, K-1\}$ . Then ,we plug the update in Algorithm 1 with NS and  $d_k$  into Equation (11) to get:

$$\phi_{s}(x_{k+1}) \leq \phi_{s}(x_{k}) + \langle \nabla \phi_{s}(x_{k}), -\beta d_{k} \rangle + \frac{L_{\phi}}{2} \| -\beta d_{k} \|^{2} 
= \phi_{s}(x_{k}) + \langle \nabla \phi_{s}(x_{k}) - \hat{\nabla} \phi_{s}(x_{k}), -\beta d_{k} \rangle - \beta \langle \hat{\nabla} \phi_{s}(x_{k}), d_{k} \rangle + \frac{L_{\phi}}{2} \beta^{2} \| d_{k} \|^{2} 
\leq \phi_{s}(x_{k}) + \frac{1}{2} \| \nabla \phi_{s}(x_{k}) - \hat{\nabla} \phi_{s}(x_{k}) \|^{2} + \frac{\beta^{2}}{2} \| d_{k} \|^{2} - \beta \langle \hat{\nabla} \phi_{s}(x_{k}), d_{k} \rangle + \frac{L_{\phi}}{2} \beta^{2} \| d_{k} \|^{2},$$
(12)

where the last inequality is due to Cauchy–Schwarz inequality. Note that  $d_k$  is computed by solving Equation (5), we leverage Theorem 5.4 to get the following inequality for every  $s \in \mathcal{S}$ :

$$\phi_s(x_{k+1}) \le \phi_s(x_k) + \frac{1}{2} \|\nabla \phi_s(x_k) - \hat{\nabla} \phi_s(x_k)\|^2 - \beta \left(\frac{1}{2r_{\text{max}}} - \frac{1}{2}\beta - \frac{L_{\phi}}{2}\beta\right) \|d_k\|^2,$$

which can be further rearranged as:

$$\beta \left( \frac{1}{2r_{\max}} - \frac{1}{2}\beta - \frac{L_{\phi}}{2}\beta \right) \|d_k\|^2 \le \phi_s(x_k) - \phi_s(x_{k+1}) + \frac{1}{2} \|\nabla \phi_s(x_k) - \hat{\nabla} \phi_s(x_k)\|^2.$$
(13)

Then, we telescope the last inequality for k from 0 to K-1, with Theorem D.1:

$$\beta \left( \frac{1}{2r_{\text{max}}} - \frac{1}{2}\beta - \frac{L_{\phi}}{2}\beta \right) \frac{1}{K} \sum_{k=0}^{K-1} \|d_{k}\|^{2}$$

$$\leq \frac{\phi_{s}(x_{0}) - \phi_{s}(x_{K})}{K} + \frac{1}{2K} \sum_{k=0}^{K-1} \|\nabla \phi_{s}(x_{k}) - \hat{\nabla} \phi_{s}(x_{k})\|^{2}$$

$$\leq \frac{\phi_{s}(x_{0}) - \phi_{s}(x_{K})}{K} + \frac{L^{2}M^{2}(1 - \alpha\mu_{g})^{2D}}{\mu_{g}^{2}}$$

$$+ \left( \frac{2L^{2}(L + \mu_{g})^{2}(1 - \alpha\mu_{g})^{D}}{\mu_{g}^{2}} + \frac{4M^{2}(\tau\mu_{g} + L\rho)^{2}}{\mu_{g}^{4}} (1 - \alpha\mu_{g})^{D-1} \right) \chi,$$
(14)

where  $\chi$  is a constant. On the other hand, we need to bound the true-gradient using the above result for hyper-gradient. Note the properties of  $\lambda_k$  for any k:  $\lambda_k^{(s)} \geq 0$ , and  $\sum_s \lambda_k^{(s)} = 1$  hold for any  $k \in \{0, 1, \dots, K-1\}$ . We first apply the triangle inequality:

$$\|\bar{d}_{k}\|^{2} \leq 2\|d_{k}\|^{2} + 2\|\bar{d}_{k} - d_{k}\|^{2}$$

$$= 2\|d_{k}\|^{2} + 2\|\sum_{s=1}^{S} \lambda_{k}^{(s)} r_{s} \left(\nabla \phi_{s}(x_{k}) - \hat{\nabla} \phi_{s}(x_{k})\right)\|^{2}$$

$$\leq 2\|d_{k}\|^{2} + 6 \max_{s} \|\nabla \phi_{s}(x_{k}) - \hat{\nabla} \phi_{s}(x_{k})\|^{2},$$
(15)

where the last inequality is due to the following reasons:

$$\| \sum_{s=1}^{S} \lambda_{k}^{(s)} r_{s} \left( \nabla \phi_{s}(x_{k}) - \hat{\nabla} \phi_{s}(x_{k}) \right) \|^{2}$$

$$= \sum_{s=1}^{S} \lambda_{k}^{(s)^{2}} r_{s}^{2} \| \nabla \phi_{s}(x_{k}) - \hat{\nabla} \phi_{s}(x_{k}) \|^{2}$$

$$+ 2 \sum_{s_{1} \neq s_{2}} \lambda_{k}^{(s_{1})} \lambda_{k}^{(s_{2})} r_{s_{1}} r_{s_{2}} \| \nabla \phi_{s_{1}}(x_{k}) - \hat{\nabla} \phi_{s_{1}}(x_{k}) \| \cdot \| \nabla \phi_{s_{2}}(x_{k}) - \hat{\nabla} \phi_{s_{2}}(x_{k}) \|$$

$$\leq \sum_{s=1}^{S} \lambda_{k}^{(s)^{2}} \| \nabla \phi_{s}(x_{k}) - \hat{\nabla} \phi_{s}(x_{k}) \|^{2}$$

$$+ 2 \sum_{s_{1} \neq s_{2}} \lambda_{k}^{(s_{1})} \lambda_{k}^{(s_{2})} \| \nabla \phi_{s_{1}}(x_{k}) - \hat{\nabla} \phi_{s_{1}}(x_{k}) \| \cdot \| \nabla \phi_{s_{2}}(x_{k}) - \hat{\nabla} \phi_{s_{2}}(x_{k}) \|$$

$$\leq \max_{s} \| \nabla \phi_{s}(x_{k}) - \hat{\nabla} \phi_{s}(x_{k}) \|^{2} \sum_{s=1}^{S} \lambda_{k}^{(s)^{2}}$$

$$+ \max_{s} \| \nabla \phi_{s}(x_{k}) - \hat{\nabla} \phi_{s}(x_{k}) \|^{2} \sum_{s_{1} \neq s_{2}} \lambda_{k}^{(s_{1})} \lambda_{k}^{(s_{2})}$$

$$\leq \max_{s} \| \nabla \phi_{s}(x_{k}) - \hat{\nabla} \phi_{s}(x_{k}) \|^{2} \sum_{s=1}^{S} \lambda_{k}^{(s)} + 2 \max_{s} \| \nabla \phi_{s}(x_{k}) - \hat{\nabla} \phi_{s}(x_{k}) \|^{2}$$

$$\leq 3 \max_{s} \| \nabla \phi_{s}(x_{k}) - \hat{\nabla} \phi_{s}(x_{k}) \|^{2},$$

$$\leq 3 \max_{s} \| \nabla \phi_{s}(x_{k}) - \hat{\nabla} \phi_{s}(x_{k}) \|^{2},$$

where the first inequality is due to the conditions of preference vector r: since  $r \in \mathbb{R}_{++}^S$ , and  $\mathbf{1}^\top r = 1$ , we know that each

element  $r_s$  is positive, and strictly less than 1. Now, we combine Equation (14) and Equation (15) to obtain:

$$\frac{\beta \left(\frac{1}{2r_{\max}} - \frac{1}{2}\beta - \frac{L_{\phi}}{2}\beta\right)}{K} \sum_{k=0}^{K-1} \|\bar{d}_{k}\|^{2} \\
\leq \frac{2\beta \left(\frac{1}{2r_{\max}} - \frac{1}{2}\beta - \frac{L_{\phi}}{2}\beta\right)}{K} \sum_{k=0}^{K-1} \|d_{k}\|^{2} + 6\beta \left(\frac{1}{2r_{\max}} - \frac{1}{2}\beta - \frac{L_{\phi}}{2}\beta\right) \max_{s,k} \|\nabla\phi_{s}(x_{k}) - \hat{\nabla}\phi_{s}(x_{k})\|^{2} \\
\leq \frac{2(\phi_{s}(x_{0}) - \phi_{s}(x_{K}))}{K} + \left(12\beta \left(\frac{1}{2r_{\max}} - \frac{1}{2}\beta - \frac{L_{\phi}}{2}\beta\right) + 2\right) \cdot \left[\left(\frac{2L^{2}(L + \mu_{g})^{2}(1 - \alpha\mu_{g})^{D}}{\mu_{q}^{2}} + \frac{4M^{2}(\tau\mu_{g} + L\rho)^{2}}{\mu_{q}^{4}}(1 - \alpha\mu_{g})^{D-1}\right)\chi + \frac{L^{2}M^{2}(1 - \alpha\mu_{g})^{2D}}{\mu_{q}^{2}}\right].$$
(17)

Therefore, selecting  $\beta = \min\{\frac{1}{2(1+L_{\phi})r_{\text{max}}}, \frac{1}{3L_{\phi}}\}$ , we attain:

$$\frac{1}{K} \sum_{k=0}^{K-1} \|\bar{d}_k\|^2 \le \frac{24r_{\max}L_{\phi}(\phi_s(x_0) - \phi_s(x_K))}{K} + (12 + 24r_{\max}L_{\phi}) \cdot \left[ \left( \frac{2L^2(L + \mu_g)^2(1 - \alpha\mu_g)^D}{\mu_q^2} + \frac{4M^2(\tau\mu_g + L\rho)^2}{\mu_q^4} (1 - \alpha\mu_g)^{D-1} \right) \chi + \frac{L^2M^2(1 - \alpha\mu_g)^{2D}}{\mu_g^2} \right].$$
(18)

As the preference r satisfies  $\mathbf{1}^{\top}r = 1$ , which implies that  $r_{\text{max}} < 1$ , thus, with this condition, we can further re-write the result as:

$$\frac{1}{K} \sum_{k=0}^{K-1} \|\bar{d}_k\|^2 \le \frac{24L_{\phi}(\phi_s(x_0) - \phi_s(x_K))}{K} + (12 + 24L_{\phi}) \cdot \left[ \left( \frac{2L^2(L + \mu_g)^2 (1 - \alpha\mu_g)^D}{\mu_g^2} + \frac{4M^2(\tau\mu_g + L\rho)^2}{\mu_g^4} (1 - \alpha\mu_g)^{D-1} \right) \chi + \frac{L^2M^2(1 - \alpha\mu_g)^{2D}}{\mu_g^2} \right].$$
(19)

In order to achieve an  $\epsilon$ -stationary Pareto point in Equation (18), we select parameters as follows:

$$\alpha \leq \frac{1}{L},$$

$$D \geq \frac{\log[(24 + 16r_{\max}L_{\phi})(2\chi(\kappa^{2}(L + \mu_{g})^{2}(1 - \alpha\mu_{g}) + \frac{4M^{2}(\tau\mu_{g} + L\rho)^{2})}{\mu_{g}^{4}}) + M^{2}\kappa^{2}(1 - \alpha\mu_{g})^{D+1})\epsilon^{-1}]}{\log(\frac{1}{1 - \alpha\mu_{g}})}$$

$$= \Theta(\kappa \log \frac{1}{\epsilon}),$$

$$K = \Theta(\kappa^{3}\epsilon^{-1}),$$

then, we have the following complexity results:

$$\begin{split} &\operatorname{Gc}(f,\epsilon) = 2K \cdot S = \mathcal{O}(\kappa^3 \epsilon^{-1} S), \\ &\operatorname{Gc}(g,\epsilon) = KD = \widetilde{\mathcal{O}}(\kappa^4 \epsilon^{-1}), \\ &\operatorname{JV}(g,\epsilon) = KD \cdot S = \widetilde{\mathcal{O}}(\kappa^4 \epsilon^{-1} S), \\ &\operatorname{HV}(g,\epsilon) = KD \cdot S = \widetilde{\mathcal{O}}(\kappa^4 \epsilon^{-1} S). \end{split}$$

Now, we prove the result of Algorithm 1 with Conjugate-Gradient (CG) method. Following that, we discuss the insight of the theoretical result.

*Proof.* (**Theorem 5.5 under option CG**) As we mentioned before, the insight of Algorithm 1 equipped with CG and NS is the same. The main distinction comes from the different control of the gap between true gradients and hyper-gradients. Here, we first

define some notations, and state a supporting lemma for the analysis. We define the following values:

$$\Gamma = 3L^{2} + \frac{3\tau^{2}M^{2}}{\mu_{g}^{2}} + 6L^{2}(1 + \sqrt{\kappa})^{2}(\kappa + \frac{\rho M}{\mu_{g}^{2}})^{2},$$

$$\delta_{D,N} = \Gamma(1 - \alpha\mu_{g})^{D} + 6L^{2}\kappa \left(\frac{\sqrt{\kappa} - 1}{\sqrt{\kappa} + 1}\right)^{2N},$$

$$\Omega = 4\beta^{2} \left(\kappa^{2} + \frac{ML}{\mu_{g}^{2}} + \frac{ML\kappa}{\mu_{g}^{2}}\right)^{2},$$

$$\chi_{0} = \|y_{0} - y^{*}(x_{0})\|^{2} + \|v_{0} - v_{0}^{*}\|^{2}.$$
(20)

The following lemma, inspired by (Ji, Yang, and Liang 2021), plays a similar role as Theorem D.1. It is worth noting that even if it shares the same form with  $Lemma\ 5$  in (Ji, Yang, and Liang 2021), the details are quite different: Since MOO with preference vector r is introduced here, the analysis should carefully handle these distinctions. This is reflected in the fact that the choices of D and N are different.

**Lemma D.2.** Suppose Theorem 5.1 and Theorem 5.2 hold. Selecting D, N large enough (will be detailed described later), for any  $s \in S$ , and  $k \in \{0, 1, ..., K-1\}$ , we have the following inequality when computing  $\hat{\nabla} \phi_s(x_k)$  using Algorithm 1 with CG:

$$\|\nabla \phi_s(x_k) - \hat{\nabla} \phi_s(x_k)\|^2 \le \delta_{D,N} \left( \left(\frac{1}{2}\right)^k \chi_0 + \Omega \sum_{j=0}^{k-1} \left(\frac{1}{2}\right)^{k-1-j} \|\nabla \phi_s(x_j)\|^2 \right).$$

We follow Equation (11) to get the similar result here for any  $s \in [S]$  and  $k \in \{0, \dots, K-1\}$ :

$$\phi_{s}(x_{k+1}) \leq \phi_{s}(x_{k}) + \langle \nabla \phi_{s}(x_{k}), -\beta d_{k} \rangle + \frac{L_{\phi}}{2} \| -\beta d_{k} \|^{2} 
= \phi_{s}(x_{k}) + \langle \nabla \phi_{s}(x_{k}) - \hat{\nabla} \phi_{s}(x_{k}), -\beta d_{k} \rangle - \beta \langle \hat{\nabla} \phi_{s}(x_{k}), d_{k} \rangle + \frac{L_{\phi}}{2} \beta^{2} \|d_{k}\|^{2} 
\leq \phi_{s}(x_{k}) + \frac{1}{2} \| \nabla \phi_{s}(x_{k}) - \hat{\nabla} \phi_{s}(x_{k}) \|^{2} + \frac{\beta^{2}}{2} \|d_{k}\|^{2} - \beta \langle \hat{\nabla} \phi_{s}(x_{k}), d_{k} \rangle + \frac{L_{\phi}}{2} \beta^{2} \|d_{k}\|^{2}$$
(21)

Plug Theorem 5.4 into this inequality and rearrange the terms, then we have:

$$\beta \left( \frac{1}{2r_{\max}} - \frac{1}{2}\beta - \frac{L_{\phi}}{2}\beta \right) \|d_k\|^2 \le \phi_s(x_k) - \phi_s(x_{k+1}) + \frac{1}{2} \|\nabla \phi_s(x_k) - \hat{\nabla} \phi_s(x_k)\|^2.$$
(22)

Now, we can apply Theorem D.2 to upper bound LHS:

$$\beta \left( \frac{1}{2r_{\text{max}}} - \frac{1}{2}\beta - \frac{L_{\phi}}{2}\beta \right) \sum_{k=0}^{K-1} \|d_{k}\|^{2}$$

$$\leq \phi_{s}(x_{0}) - \phi_{s}(x_{K}) + \frac{1}{2}\delta_{D,N} \sum_{k=0}^{K-1} \left( \left( \frac{1}{2} \right)^{k} \chi_{0} + \Omega \sum_{j=0}^{K-1} \left( \frac{1}{2} \right)^{k-1-j} \|\nabla \phi_{s}(x_{j})\|^{2} \right)$$

$$\leq \phi_{s}(x_{0}) - \phi_{s}(x_{K}) + \delta_{D,N}\chi_{0} + \delta_{D,N}\Omega \sum_{k=0}^{K-1} \sum_{j=0}^{K-1} \left( \frac{1}{2} \right)^{k-j} \|\nabla \phi_{s}(x_{j})\|^{2}$$

$$\leq \phi_{s}(x_{0}) - \phi_{s}(x_{K}) + \delta_{D,N}\chi_{0} + \delta_{D,N}\Omega \sum_{k=0}^{K-1} \|\nabla \phi_{s}(x_{k})\|^{2}$$

$$\leq \phi_{s}(x_{0}) - \phi_{s}(x_{K}) + \delta_{D,N}\chi_{0} + 2KM^{2}\delta_{D,N}\Omega(\kappa^{2} + 1).$$

$$(23)$$

where the last inequality is due to Equation (35). Therefore, select  $\beta = \min\{\frac{1}{2(1+L_{\phi})r_{\max}}, \frac{1}{3L_{\phi}}\}$ , then we have:

$$\frac{1}{K} \sum_{k=0}^{K-1} \|d_k\|^2 \le \frac{12r_{\max} L_{\phi} \left(\phi_s(x_0) - \phi_s(x_K) + \delta_{D,N} \chi_0\right)}{K} + 24r_{\max} L_{\phi} M^2 \delta_{D,N} \Omega(\kappa^2 + 1). \tag{24}$$

Now, by Equation (15), we have:

$$\frac{1}{K} \sum_{k=0}^{K-1} \|\bar{d}_{k}\|^{2} 
\leq \frac{2}{K} \sum_{k=0}^{K-1} \|d_{k}\|^{2} + 6 \max_{s,k} \|\nabla \phi_{s}(x_{k}) - \hat{\nabla} \phi_{s}(x_{k})\|^{2} 
\leq \frac{2}{K} \sum_{k=0}^{K-1} \|d_{k}\|^{2} + 6 \delta_{D,N} \max_{s,k} \left( \left(\frac{1}{2}\right)^{k} \chi_{0} + \Omega \sum_{j=0}^{k-1} \left(\frac{1}{2}\right)^{k-1-j} \|\nabla \phi_{s}(x_{j})\|^{2} \right) 
\leq \frac{2}{K} \sum_{k=0}^{K-1} \|d_{k}\|^{2} + 6 \delta_{D,N} \chi_{0} + 24 M^{2} \delta_{D,N} \Omega(\kappa^{2} + 1) 
\leq \frac{12 r_{\max} L_{\phi} \left(\phi_{s}(x_{0}) - \phi_{s}(x_{K}) + \delta_{D,N} \chi_{0}\right)}{K} + 24 (r_{\max} L_{\phi} + 1) M^{2} \delta_{D,N} \Omega(\kappa^{2} + 1) + 6 \delta_{D,N} \chi_{0}.$$

The desired result can be attained since we have  $\kappa^2 + 1 \le \sqrt{\Omega}$ . In order to achieve an  $\epsilon$ -stationary Pareto point, we select parameters as follows:

$$\begin{split} \alpha & \leq \frac{1}{L}, \\ D & \geq \frac{\log[24\Gamma(\chi_0 + 4M^2\Omega(\kappa^2 + 1)(r_{\max}L_{\phi} + 1))\epsilon^{-1}]}{\log(\frac{1}{1 - \alpha\mu_g})} = \Theta(\kappa\log\frac{1}{\epsilon}), \\ N & \geq \frac{\log[144L^2\kappa(\chi_0 + 4M^2\Omega(\kappa^2 + 1)(r_{\max}L_{\phi} + 1))\epsilon^{-1}]}{2\log(\frac{\sqrt{\kappa} + 1}{\sqrt{\kappa} - 1})} = \Theta(\sqrt{\kappa}\log\frac{1}{\epsilon}), \\ K & = \Theta(\kappa^3\epsilon^{-1}), \end{split}$$

then, we have the following complexity results:

$$\begin{split} &\operatorname{Gc}(f,\epsilon) = 2K \cdot S = \mathcal{O}(\kappa^3 \epsilon^{-1} S), \\ &\operatorname{Gc}(g,\epsilon) = KD = \widetilde{\mathcal{O}}(\kappa^4 \epsilon^{-1}), \\ &\operatorname{JV}(g,\epsilon) = K \cdot S = \mathcal{O}(\kappa^3 \epsilon^{-1} S), \\ &\operatorname{HV}(g,\epsilon) = KN \cdot S = \widetilde{\mathcal{O}}(\kappa^{3.5} \epsilon^{-1} S). \end{split}$$

We observe that Algorithm 1 using CG achieves the same convergence rate as Algorithm 1 with the NS approximation. Furthermore, as demonstrated in complexities of two methods, the oracle complexity of the CG method is even more favorable. However, we claim that both approaches offer distinct advantages in different aspects: on the one hand, CG achieves greater efficiency in terms of oracle complexity; on the other hand, (Xiao and Ji 2023) highlights that the NS approximation is more communication-efficient in federated settings.

### D.4 Proof of Theorem 5.7

*Proof.* For stochastic case, we first introduce some notations and supporting lemmas for the proof. Specifically, we define:

$$\theta = 2\left(\frac{L - \mu_g}{L + \mu_g}\right)^{2D},$$

$$\nu = \left(L + \frac{L}{\mu_g} + \frac{M\tau}{\mu_g} + \frac{LM\rho}{\mu_g^2}\right)^2,$$

$$\gamma = 8\theta \frac{\beta^2 L^2 \nu}{\mu_g^2} \frac{r_{\text{max}}}{1 - r_{\text{max}}},$$

$$\chi = \frac{4L^2 M^2}{\mu_g^2 D_g} + \left(\frac{8L^2}{\mu_g^2} + 2\right) \frac{M^2}{D_f} + \frac{16\eta^2 L^4 M^2}{B\mu_g^2} + \frac{16L^2 M^2 (1 - \eta \mu_g)^{2Q}}{\mu_g^2}.$$
(26)

We first introduce two lemmas. The first lemma is inspired by (Ji, Yang, and Liang 2021):

**Lemma D.3.** Suppose Theorem 5.1, Theorem 5.2, and Theorem 5.3 hold. Then, we have:

$$\mathbb{E} \|\nabla \phi_s(x_k) - \hat{\nabla} \phi_s(x_k)\|^2 \le \chi + \nu \mathbb{E} \|y_k^D - y^*(x_k)\|^2.$$

The second lemma is stated and proved as follows:

**Lemma D.4.** Suppose Theorem 5.1, Theorem 5.2, and Theorem 5.3 hold. Selecting D such that  $\theta < 1$  and setting  $\alpha = \frac{2}{L + \mu_g}$ , we have the following inequality for any  $s \in [S]$ :

$$\mathbb{E}\|y_k^D - y^*(x_k)\|^2 \le \gamma^k \mathbb{E}\|y_0 - y^*(x_0)\|^2 + \frac{\gamma}{4\nu} \sum_{j=0}^{k-1} \gamma^{k-1-j} \mathbb{E}\|\nabla \phi_s(x_j)\|^2 + \frac{1}{1-\gamma} \cdot \left(\frac{\sigma^2}{L\mu_g T} + \frac{\gamma\chi}{4\nu}\right).$$

*Proof.* From (Ji, Yang, and Liang 2021), we have the following inequality when selecting  $\alpha = \frac{2}{L + \mu_g}$ :

$$\mathbb{E}\|y_k^D - y^*(x_k)\|^2 \le \left(\frac{L - \mu_g}{L + \mu_g}\right)^{2D} \mathbb{E}\|y_{k-1}^D - y^*(x_k)\|^2 + \frac{\sigma^2}{L\mu_g T}.$$
 (27)

To find the relationship between  $\mathbb{E}\|y_k^D - y^*(x_k)\|^2$  and  $\mathbb{E}\|y_{k-1}^D - y^*(x_{k-1})\|^2$ , we focus on the first term of the RHS in the last inequality. For any  $s \in [S]$ , we have:

$$\begin{split} & \mathbb{E}\|y_{k-1}^{D} - y^{*}(x_{k})\|^{2} \\ & \stackrel{(a)}{\leq} 2\mathbb{E}\|y_{k-1}^{D} - y^{*}(x_{k-1})\|^{2} + \frac{2\beta^{2}L^{2}}{\mu_{g}^{2}} \mathbb{E}\|d_{k-1}\|^{2} \\ & \stackrel{(b)}{\leq} 2\mathbb{E}\|y_{k-1}^{D} - y^{*}(x_{k-1})\|^{2} + \frac{2\beta^{2}L^{2}}{\mu_{g}^{2}} \frac{r_{\max}}{1 - r_{\max}} \mathbb{E}\|\hat{\nabla}\phi_{s}(x_{k-1})\|^{2} \\ & \stackrel{(c)}{\leq} 2\mathbb{E}\|y_{k-1}^{D} - y^{*}(x_{k-1})\|^{2} + \frac{4\beta^{2}L^{2}}{\mu_{g}^{2}} \frac{r_{\max}}{1 - r_{\max}} \mathbb{E}\|\nabla\phi_{s}(x_{k-1})\|^{2} + \frac{4\beta^{2}L^{2}}{\mu_{g}^{2}} \frac{r_{\max}}{1 - r_{\max}} \mathbb{E}\|\hat{\nabla}\phi_{s}(x_{k-1})\|^{2} + \frac{4\beta^{2}L^{2}}{\mu_{g}^{2}} \frac{r_{\max}}{1 - r_{\max}} \mathbb{E}\|\hat{\nabla}\phi_{s}(x_{k-1})\|^{2} + \frac{4\beta^{2}L^{2}}{\mu_{g}^{2}} \frac{r_{\max}}{1 - r_{\max}} (\chi + \nu \mathbb{E}\|y_{k-1}^{D} - y^{*}(x_{k-1})\|^{2}) \\ & = \left(2 + \frac{4\beta^{2}L^{2}\nu}{\mu_{g}^{2}} \frac{r_{\max}}{1 - r_{\max}}\right) \mathbb{E}\|y_{k-1}^{D} - y^{*}(x_{k-1})\|^{2} + \frac{4\beta^{2}L^{2}}{\mu_{g}^{2}} \frac{r_{\max}}{1 - r_{\max}} (\mathbb{E}\|\nabla\phi_{s}(x_{k-1})\|^{2} + \chi). \end{split}$$

where (a) is from (Ghadimi and Wang 2018), (b) is due to Theorem 5.4, (c) leverages triangle inequality, (d) applies Theorem D.3. Therefore, we combine Equations (27) and (28) to get:

$$\mathbb{E}\|y_{k}^{D} - y^{*}(x_{k})\|^{2}$$

$$\leq \gamma \mathbb{E}\|y_{k-1}^{D} - y^{*}(x_{k-1})\|^{2} + \frac{\gamma}{4\nu} (\mathbb{E}\|\nabla\phi_{s}(x_{k-1})\|^{2} + \chi) + \frac{\sigma^{2}}{L\mu_{g}T}$$

$$\leq \gamma^{k} \mathbb{E}\|y_{0} - y^{*}(x_{0})\|^{2} + \frac{\gamma}{4\nu} \sum_{j=0}^{k-1} \gamma^{k-1-j} \mathbb{E}\|\nabla\phi_{s}(x_{j})\|^{2} + \frac{1}{1-\gamma} \cdot \left(\frac{\sigma^{2}}{L\mu_{g}T} + \frac{\gamma\chi}{4\nu}\right),$$
(29)

where the last inequality is due to telescoping, and this ends the proof of lemma.

In the beginning the proof process for Theorem 5.7, we give the closed form of  $v_k^{(s),Q}$  for any s and k:

$$v_k^{(s),Q} = \eta \sum_{q=-1}^{Q-1} \prod_{j=Q-q}^{Q} (I - \eta \nabla_y^2 G(x_k, y_k^D; \mathcal{B}_j)) v_k^{(s),0}.$$
 (30)

Now, we leverage the descent lemma which comes from Theorem 5.2 to get the following result for each  $s \in [S]$ , and  $k \in [K]$ :

$$\phi_{s}(x_{k+1}) \leq \phi_{s}(x_{k}) + \langle \nabla \phi_{s}(x_{k}), -\beta d_{k} \rangle + \frac{L_{\phi}}{2} \| -\beta d_{k} \|^{2} 
= \phi_{s}(x_{k}) + \langle \nabla \phi_{s}(x_{k}) - \hat{\nabla} \phi_{s}(x_{k}), -\beta d_{k} \rangle - \beta \langle \hat{\nabla} \phi_{s}(x_{k}), d_{k} \rangle + \frac{L_{\phi}}{2} \beta^{2} \| d_{k} \|^{2} 
\leq \phi_{s}(x_{k}) + \frac{1}{2} \| \nabla \phi_{s}(x_{k}) - \hat{\nabla} \phi_{s}(x_{k}) \|^{2} + \frac{\beta^{2}}{2} \| d_{k} \|^{2} - \beta \langle \hat{\nabla} \phi_{s}(x_{k}), d_{k} \rangle + \frac{L_{\phi}}{2} \beta^{2} \| d_{k} \|^{2}.$$
(31)

Note that the update direction  $d_k = \hat{\nabla}\Phi(x_k)\mathrm{diag}(r)\lambda_k$  satisfies Theorem 5.4, thus, we have:

$$\phi_s(x_{k+1}) \le \phi_s(x_k) + \frac{1}{2} \|\nabla \phi_s(x_k) - \hat{\nabla} \phi_s(x_k)\|^2 - \beta \left(\frac{1}{2r_{\text{max}}} - \frac{1}{2}\beta - \frac{L_\phi}{2}\beta\right) \|d_k\|^2.$$
 (32)

Taking expectation on both sides, and rearranging the inequality, we attain:

$$\beta \left( \frac{1}{2r_{\max}} - \frac{1}{2}\beta - \frac{L_{\phi}}{2}\beta \right) \mathbb{E}\|d_k\|^2 \le \mathbb{E}(\phi_s(x_k)) - \mathbb{E}(\phi_s(x_{k+1})) + \frac{1}{2}\mathbb{E}\|\nabla\phi_s(x_k) - \hat{\nabla}\phi_s(x_k)\|^2.$$
 (33)

Now, we plug Theorems D.3 and D.4 into the RHS of this inequality:

$$\beta \left( \frac{1}{2r_{\max}} - \frac{1}{2}\beta - \frac{L_{\phi}}{2}\beta \right) \mathbb{E} \|d_{k}\|^{2}$$

$$\leq \mathbb{E}(\phi_{s}(x_{k})) - \mathbb{E}(\phi_{s}(x_{k+1})) + \frac{1}{2}(\chi + \nu \mathbb{E} \|y_{k}^{D} - y^{*}(x_{k})\|^{2})$$

$$\leq \mathbb{E}(\phi_{s}(x_{k})) - \mathbb{E}(\phi_{s}(x_{k+1})) + \frac{\nu}{2}\gamma^{k}\mathbb{E} \|y_{0} - y^{*}(x_{0})\|^{2} + \frac{1}{8}\sum_{i=0}^{K-1}\gamma^{k-j}\mathbb{E} \|\nabla\phi_{s}(x_{j})\|^{2} + \left(\frac{4+\gamma}{8}\chi + \frac{\nu}{1-\gamma}\frac{\sigma^{2}}{2L\mu_{g}T}\right).$$
(34)

Note the following facts:

$$\mathbb{E}\|\nabla\phi_{s}(x_{k})\|^{2} \\
=\mathbb{E}\|\nabla_{x}f^{(s)}(x_{k},y^{*}(x_{k})) - \nabla_{xy}^{2}g(x_{k},y^{*}(x_{k}))v_{k}^{*}\|^{2} \\
=\mathbb{E}\|\nabla_{x}f^{(s)}(x_{k},y^{*}(x_{k})) - \nabla_{xy}^{2}g(x_{k},y^{*}(x_{k}))(\nabla_{y}^{2}g(x_{k},y^{*}(x_{k})))^{-1}\nabla_{y}f(x_{k},y^{*}(x_{k}))\|^{2} \\
\leq 2\mathbb{E}\|\nabla_{x}f^{(s)}(x_{k},y^{*}(x_{k}))\|^{2} + 2\mathbb{E}(\|\nabla_{xy}^{2}g(x_{k},y^{*}(x_{k}))\|^{2} \cdot \|(\nabla_{y}^{2}g(x_{k},y^{*}(x_{k})))^{-1}\nabla_{y}f(x_{k},y^{*}(x_{k}))\|^{2}) \\
\leq 2M^{2}(1 + \frac{L^{2}}{\mu_{g}^{2}}), \tag{35}$$

holds for each s and k, which is due to Theorem 5.1, Theorem 5.2 and Theorem 5.3, and

$$\sum_{k=1}^{K} \sum_{j=0}^{k-1} \gamma^{k-j-1} \mathbb{E} \|\nabla \phi_s(x_j)\|^2 \le \frac{1}{1-\gamma} \sum_{k=1}^{K} \mathbb{E} \|\nabla \phi_s(x_k)\|^2.$$

Thus, we telescope Equation (34) for k from 1 to K, then we have:

$$\beta \left( \frac{1}{2r_{\max}} - \frac{1}{2}\beta - \frac{L_{\phi}}{2}\beta \right) \frac{1}{K} \sum_{k=1}^{K} \mathbb{E} \|d_{k}\|^{2}$$

$$\leq \frac{\mathbb{E}(\phi_{s}(x_{0})) - \mathbb{E}(\phi_{s}(x_{K}))}{K} + \frac{\nu\gamma}{2(1-\gamma)} \mathbb{E} \|y_{0} - y^{*}(x_{0})\|^{2} + \left( \frac{4+\gamma}{8}\chi + \frac{\nu}{1-\gamma} \frac{\sigma^{2}}{2L\mu_{q}T} \right) + \frac{\gamma M^{2}(1+\kappa^{2})}{4(1-\gamma)}.$$
(36)

Select  $\beta \leq \frac{1}{2(1+L_\phi)r_{\max}}$ , then we have  $\frac{1}{2r_{\max}}-\frac{1}{2}\beta-\frac{L_\phi}{2}\beta \geq \frac{1}{4r_{\max}}$ . Therefore, we have:

$$\frac{1}{K} \sum_{k=1}^{K} \mathbb{E} \|d_{k}\|^{2} \leq \frac{4r_{\max}}{\beta}.$$

$$\left[ \frac{\mathbb{E}(\phi_{s}(x_{0})) - \mathbb{E}(\phi_{s}(x_{K}))}{K} + \frac{\nu\gamma}{2(1-\gamma)} \mathbb{E} \|y_{0} - y^{*}(x_{0})\|^{2} + \left(\frac{4+\gamma}{8}\chi + \frac{\nu}{1-\gamma}\frac{\sigma^{2}}{2L\mu_{g}T}\right) + \frac{\gamma M^{2}(1+\kappa^{2})}{4(1-\gamma)} \right].$$
(37)

To upper bound  $\frac{1}{K} \sum_{k=1}^{K} \mathbb{E} \|\bar{d}_k\|^2$ , we bridge the final result using triangle inequality:

$$\mathbb{E}\|\bar{d}_{k}\|^{2} \leq 2\mathbb{E}\|d_{k}\|^{2} + 2\mathbb{E}\|\bar{d}_{k} - d_{k}\|^{2}$$

$$= 2\mathbb{E}\|d_{k}\|^{2} + 2\mathbb{E}\|\sum_{s=1}^{S} \lambda_{k}^{(s)} r_{s} \left(\nabla \phi_{s}(x_{k}) - \hat{\nabla} \phi_{s}(x_{k})\right)\|^{2}$$

$$= 2\mathbb{E}\|d_{k}\|^{2} + 2\mathbb{E}\left[\sum_{s=1}^{S} \lambda_{k}^{(s)^{2}} r_{s}^{2} \|\nabla \phi_{s}(x_{k}) - \hat{\nabla} \phi_{s}(x_{k})\|^{2}$$

$$+ 2\sum_{s_{1} \neq s_{2}} \lambda_{k}^{(s_{1})} \lambda_{k}^{(s_{2})} r_{s_{1}} r_{s_{2}} \|\nabla \phi_{s_{1}}(x_{k}) - \hat{\nabla} \phi_{s_{1}}(x_{k})\| \cdot \|\nabla \phi_{s_{2}}(x_{k}) - \hat{\nabla} \phi_{s_{2}}(x_{k})\|\right]$$

$$\leq 2\mathbb{E}\|d_{k}\|^{2} + 2\mathbb{E}\left[\max_{s} \|\nabla \phi_{s}(x_{k}) - \hat{\nabla} \phi_{s}(x_{k})\|^{2} \sum_{s=1}^{S} \lambda_{k}^{(s)^{2}}\right]$$

$$+ 4\mathbb{E}\left[\max_{s} \|\nabla \phi_{s}(x_{k}) - \hat{\nabla} \phi_{s}(x_{k})\|^{2} 2 \sum_{s_{1} \neq s_{2}} \lambda_{k}^{(s_{1})} \lambda_{k}^{(s_{2})}\right]$$

$$\leq 2\mathbb{E}\|d_{k}\|^{2} + 6\mathbb{E}\left(\max_{s} \|\nabla \phi_{s}(x_{k}) - \hat{\nabla} \phi_{s}(x_{k})\|^{2}\right).$$

$$(38)$$

Thus.

$$\frac{1}{K} \sum_{k=1}^{K} \mathbb{E} \|\bar{d}_k\|^2 \le \frac{2}{K} \sum_{k=1}^{K} \mathbb{E} \|d_k\|^2 + 6\mathbb{E} \left( \max_{s,k} \|\nabla \phi_s(x_k) - \hat{\nabla} \phi_s(x_k)\|^2 \right). \tag{39}$$

Therefore, we combine Theorems D.3 and D.4 and Equations (35) and (37) together to get:

$$\begin{split} &\frac{1}{K}\sum_{k=1}^{K}\mathbb{E}\|\bar{d}_{k}\|^{2} \\ &\leq \frac{2}{K}\sum_{k=1}^{K}\mathbb{E}\|d_{k}\|^{2} + 6\mathbb{E}\left(\max_{s,k}\|\nabla\phi_{s}(x_{k}) - \hat{\nabla}\phi_{s}(x_{k})\|^{2}\right) \\ &\leq \frac{8r_{\max}}{\beta}\left[\frac{\mathbb{E}(\phi_{s}(x_{0})) - \mathbb{E}(\phi_{s}(x_{K}))}{K} + \frac{\nu\gamma}{2(1-\gamma)}\mathbb{E}\|y_{0} - y^{*}(x_{0})\|^{2} + \left(\frac{4+\gamma}{8}\chi + \frac{\nu}{1-\gamma}\frac{\sigma^{2}}{2L\mu_{g}T}\right) + \frac{\gamma M^{2}(1+\kappa^{2})}{4(1-\gamma)}\right] \\ &+ 6\chi + 6\nu\max_{k,s}\left(\gamma^{k}\mathbb{E}\|y_{0} - y^{*}(x_{0})\|^{2} + \frac{\gamma}{4\nu}\sum_{j=0}^{k-1}\gamma^{k-1-j}\mathbb{E}\|\nabla\phi_{s}(x_{j})\|^{2} + \frac{1}{1-\gamma}\cdot\left(\frac{\sigma^{2}}{L\mu_{g}T} + \frac{\gamma\chi}{4\nu}\right)\right) \\ &\leq \frac{8r_{\max}}{\beta}\left[\frac{\mathbb{E}(\phi_{s}(x_{0})) - \mathbb{E}(\phi_{s}(x_{K}))}{K} + \frac{\nu\gamma}{2(1-\gamma)}\mathbb{E}\|y_{0} - y^{*}(x_{0})\|^{2} + \left(\frac{4+\gamma}{8}\chi + \frac{\nu}{1-\gamma}\frac{\sigma^{2}}{2L\mu_{g}T}\right) + \frac{\gamma M^{2}(1+\kappa^{2})}{4(1-\gamma)}\right] \\ &+ 6\chi + 6\nu\gamma\mathbb{E}\|y_{0} - y^{*}(x_{0})\|^{2} + \frac{6\nu}{1-\gamma}\cdot\left(\frac{\sigma^{2}}{L\mu_{g}T} + \frac{\gamma\chi}{4\nu}\right) + \frac{3\gamma}{2(1-\gamma)}\max_{k,s}\mathbb{E}\|\nabla\phi_{s}(x_{k})\|^{2} \\ &\leq \frac{8r_{\max}}{\beta}\left[\frac{\mathbb{E}(\phi_{s}(x_{0})) - \mathbb{E}(\phi_{s}(x_{K}))}{K} + \frac{\nu\gamma}{2(1-\gamma)}\mathbb{E}\|y_{0} - y^{*}(x_{0})\|^{2} + \left(\frac{4+\gamma}{8}\chi + \frac{\nu}{1-\gamma}\frac{\sigma^{2}}{2L\mu_{g}T}\right) + \frac{\gamma M^{2}(1+\kappa^{2})}{4(1-\gamma)}\right] \\ &+ 6\chi + 6\nu\gamma\mathbb{E}\|y_{0} - y^{*}(x_{0})\|^{2} + \frac{6\nu}{1-\gamma}\cdot\left(\frac{\sigma^{2}}{L\mu_{g}T} + \frac{\gamma\chi}{4\nu}\right) + \frac{3M^{2}(\kappa^{2}+1)\gamma}{1-\gamma}. \end{split}$$

We select  $\beta = \min\{\frac{1}{2(1+L_{\phi})r_{\max}}, \frac{1}{3L_{\phi}}\}$ , then this result can be further written using order notations as follows:

$$\frac{1}{K} \sum_{k=1}^{K} \mathbb{E} \|\bar{d}_{k}\|^{2} \leq \mathcal{O}\left(\frac{L_{\phi}}{K} + \frac{\kappa^{8}\sigma^{2}}{T} + \frac{\kappa^{5}}{D_{g}} + \frac{\kappa^{5}}{D_{f}} + \frac{\kappa^{5}}{B} + \kappa^{5}(1 - \eta\mu_{g})^{2Q}\right) + \gamma \cdot \left(6\nu + \frac{12L_{\phi}r_{\max}\nu}{1 - \gamma}\right) \mathbb{E} \|y_{0} - y^{*}(x_{0})\|^{2} + \gamma \cdot \frac{3M^{2}(\kappa^{2} + 1)}{1 - \gamma}\left(1 + 2L_{\phi}r_{\max}\right). \tag{41}$$

#### Algorithm 4: Non-Preference Deterministic Algorithm

```
1: Input: The numbers of iteration K, D, N, initialization values x_0, y_0, v_0, and step-sizes \alpha, \beta.

2: for k = 0, 1, \ldots, K - 1 do

3: Set y_k^0 = y_{k-1}^D if k > 0 and y_0 otherwise.

4: for t = 1, 2, \ldots, D do

5: Update y_k^t = y_k^{t-1} - \alpha \nabla_y g(x_k, y_k^{t-1}).

6: end for

7: for s \in [S] do

8: Compute \hat{\nabla} \phi_s(x_k) according to Equation (4).

9: end for

10: Compute \lambda_k = \arg\min_{\lambda} \|\lambda^\top \hat{\nabla} \Phi(x_k)\|^2 s.t. \sum_{s=1}^S \lambda_k^{(s)} = 1, \lambda_k^{(s)} \geq 0, \forall s \in [S].

11: Update x_{k+1} = x_k - \beta \sum_{s=1}^S \lambda_k^{(s)} \hat{\nabla} \phi_s(x_k).

12: end for
```

In order to attain an  $\epsilon$ -stationary Pareto point, we select parameters as follows:

$$\alpha = \frac{2}{L + \mu_g}, \eta \le \frac{1}{L}, K = \Theta(\frac{\kappa^3}{\epsilon}), D = \Theta(\kappa \log(\epsilon^{-1})), Q = \Theta(\kappa \log(\kappa^2 \epsilon^{-1})),$$

$$T = \Theta(\frac{\kappa^8}{\epsilon}), D_f = \Theta(\frac{\kappa^5}{\epsilon}), D_g = \Theta(\frac{\kappa^5}{\epsilon}), B = \Theta(\frac{\kappa^5}{\epsilon}),$$

then, the complexity result is:

$$\begin{split} &\operatorname{Gc}(f,\epsilon) = KD_f \cdot S = \mathcal{O}(\kappa^8 \epsilon^{-2} S), \\ &\operatorname{Gc}(g,\epsilon) = KDT = \widetilde{\mathcal{O}}(\kappa^{12} \epsilon^{-2}), \\ &\operatorname{JV}(g,\epsilon) = KD_g \cdot S = \mathcal{O}(\kappa^8 \epsilon^{-2} S), \\ &\operatorname{HV}(g,\epsilon) = \frac{KBQ}{\eta \mu_g} \cdot S = \widetilde{\mathcal{O}}(\kappa^9 \epsilon^{-2} S). \end{split}$$

### D.5 Theoretical result for non-preference scenario

In this section, we present the algorithm and theoretical results for the non-preference scenario, where the user preference r is either not provided or not critical. This aligns precisely with the fourth type of MOO philosophy discussed in Section 3, where our objective is to identify an arbitrary Pareto stationary point regardless of the preference. We begin by introducing the algorithm, followed by an analysis that demonstrates how this scenario serves as a special case of the main theories of WC-MHGD discussed in Section 5.

As shown in Algorithm 4, we only focus on the deterministic case for brevity. We have previously discussed that the choice between CG and NS primarily affects the gap between true gradients and hyper-gradients. Therefore, we only consider the algorithm equipped with the NS approximation. The key difference between Algorithm 4 and Algorithm 1 lies in the computation of  $\lambda_k$ , for any  $k \in \{0, \dots, K-1\}$ . Since the preference r is not a concern in this scenario, the primal MGDA can be utilized to determine  $\lambda_k$  and  $d_k$ . We state and prove the theoretical result as follows:

**Theorem D.5.** Suppose Theorem 5.1 and Theorem 5.2 hold. For any  $\epsilon > 0$ , when selecting  $\alpha \leq \frac{1}{L}$ ,  $\beta = \min\{\frac{1}{2(1+L_{\phi})r_{\max}}, \frac{1}{3L_{\phi}}\}$ ,  $D \geq \Theta(\kappa \log \frac{1}{\epsilon})$ , and  $K = \Theta(\kappa^3 \epsilon^{-1})$ , Algorithm 4 with NS approximation satisfies:

$$\frac{1}{K} \sum_{k=0}^{K-1} \|\bar{d}_k\|^2 \le \frac{8L_{\phi}(\phi_s(x_0) - \phi_s(x_K))}{K} + (12 + 8L_{\phi}) \cdot \left[ \left( \frac{2L^2(L + \mu_g)^2 (1 - \alpha\mu_g)^D}{\mu_q^2} + \frac{4M^2(\tau\mu_g + L\rho)^2}{\mu_q^4} (1 - \alpha\mu_g)^{D-1} \right) \chi + \frac{L^2M^2(1 - \alpha\mu_g)^{2D}}{\mu_q^2} \right].$$

where  $\chi$  is a positive constant, and the detailed form of D is:

$$D \ge \frac{\log[(24 + 16L_{\phi})(2\chi(\kappa^{2}(L + \mu_{g})^{2}(1 - \alpha\mu_{g}) + \frac{4M^{2}(\tau\mu_{g} + L\rho)^{2})}{\mu_{g}^{4}}) + M^{2}\kappa^{2}(1 - \alpha\mu_{g})^{D+1})\epsilon^{-1}]}{\log(\frac{1}{1 - \alpha\mu_{g}})}$$

$$= \Theta(\kappa \log \frac{1}{\epsilon}).$$

To achieve an  $\epsilon$ -Pareto stationary point, i.e., to let  $\frac{1}{K} \sum_{k=0}^{K-1} \|\bar{d}_k\|^2 \leq \epsilon$ , the oracle complexities are:

$$\begin{split} & \operatorname{Gc}(f,\epsilon) = \mathcal{O}(\kappa^3 \epsilon^{-1} S), \operatorname{Gc}(g,\epsilon) = \widetilde{\mathcal{O}}(\kappa^4 \epsilon^{-1}), \\ & \operatorname{JV}(g,\epsilon) = \widetilde{\mathcal{O}}(\kappa^4 \epsilon^{-1} S), \operatorname{HV}(g,\epsilon) = \widetilde{\mathcal{O}}(\kappa^4 \epsilon^{-1} S). \end{split}$$

*Proof.* The main process is similar to the proof of Theorem 5.5. By Equations (11) and (12), we attain:

$$\beta \left( 1 - \frac{1}{2}\beta - \frac{L_{\phi}}{2}\beta \right) \|d_k\|^2 \le \phi_s(x_k) - \phi_s(x_{k+1}) + \frac{1}{2} \|\nabla \phi_s(x_k) - \hat{\nabla} \phi_s(x_k)\|^2. \tag{42}$$

Note that we leverage the property of MGDA instead of our Theorem 5.4 here, i.e., the descent direction  $d_k$  derived by MGDA satisfies the following inequality:

$$\langle \hat{\nabla} \phi_s(x_k), d_k \rangle \ge ||d_k||^2. \tag{43}$$

Then, we telescope the last inequality for k from 0 to K-1, with Theorem D.1:

$$\beta \left(1 - \frac{1}{2}\beta - \frac{L_{\phi}}{2}\beta\right) \frac{1}{K} \sum_{k=0}^{K-1} \|d_{k}\|^{2}$$

$$\leq \frac{\phi_{s}(x_{0}) - \phi_{s}(x_{K})}{K} + \frac{1}{2K} \sum_{k=0}^{K-1} \|\nabla\phi_{s}(x_{k}) - \hat{\nabla}\phi_{s}(x_{k})\|^{2}$$

$$\leq \frac{\phi_{s}(x_{0}) - \phi_{s}(x_{K})}{K} + \frac{L^{2}M^{2}(1 - \alpha\mu_{g})^{2D}}{\mu_{g}^{2}}$$

$$+ \left(\frac{2L^{2}(L + \mu_{g})^{2}(1 - \alpha\mu_{g})^{D}}{\mu_{g}^{2}} + \frac{4M^{2}(\tau\mu_{g} + L\rho)^{2}}{\mu_{g}^{4}}(1 - \alpha\mu_{g})^{D-1}\right)\chi,$$
(44)

where  $\chi$  is a constant. Using Equation (15), we have:

$$\frac{\beta \left(1 - \frac{1}{2}\beta - \frac{L_{\phi}}{2}\beta\right)}{K} \sum_{k=0}^{K-1} \|\bar{d}_{k}\|^{2} 
\leq \frac{2\beta \left(1 - \frac{1}{2}\beta - \frac{L_{\phi}}{2}\beta\right)}{K} \sum_{k=0}^{K-1} \|d_{k}\|^{2} + 6\beta \left(1 - \frac{1}{2}\beta - \frac{L_{\phi}}{2}\beta\right) \max_{s,k} \|\nabla\phi_{s}(x_{k}) - \hat{\nabla}\phi_{s}(x_{k})\|^{2} 
\leq \frac{2(\phi_{s}(x_{0}) - \phi_{s}(x_{K}))}{K} + \left(12\beta \left(1 - \frac{1}{2}\beta - \frac{L_{\phi}}{2}\beta\right) + 2\right) \cdot \left[\left(\frac{2L^{2}(L + \mu_{g})^{2}(1 - \alpha\mu_{g})^{D}}{\mu_{g}^{2}} + \frac{4M^{2}(\tau\mu_{g} + L\rho)^{2}}{\mu_{g}^{4}}(1 - \alpha\mu_{g})^{D-1}\right)\chi + \frac{L^{2}M^{2}(1 - \alpha\mu_{g})^{2D}}{\mu_{g}^{2}}\right].$$
(45)

Selecting  $\beta = \min\{\frac{3}{2(1+L_{\phi})}, \frac{1}{L_{\phi}}\}$ , we attain:

$$\frac{1}{K} \sum_{k=0}^{K-1} \|\bar{d}_k\|^2 \le \frac{8L_{\phi}(\phi_s(x_0) - \phi_s(x_K))}{K} + (12 + 8L_{\phi}) \cdot \left[ \left( \frac{2L^2(L + \mu_g)^2 (1 - \alpha\mu_g)^D}{\mu_g^2} + \frac{4M^2(\tau\mu_g + L\rho)^2}{\mu_g^4} (1 - \alpha\mu_g)^{D-1} \right) \chi + \frac{L^2M^2 (1 - \alpha\mu_g)^{2D}}{\mu_g^2} \right].$$
(46)

In order to achieve an  $\epsilon$ -accurate stationary point, we select parameters as follows:

$$\alpha \leq \frac{1}{L},$$

$$D \geq \frac{\log[(24 + 16L_{\phi})(2\chi(\kappa^{2}(L + \mu_{g})^{2}(1 - \alpha\mu_{g}) + \frac{4M^{2}(\tau\mu_{g} + L\rho)^{2})}{\mu_{g}^{4}}) + M^{2}\kappa^{2}(1 - \alpha\mu_{g})^{D+1})\epsilon^{-1}]}{\log(\frac{1}{1 - \alpha\mu_{g}})}$$

$$= \Theta(\kappa \log \frac{1}{\epsilon}),$$

$$K = \Theta(\kappa^{3}\epsilon^{-1}),$$

then, we have the following complexity results:

$$\begin{split} &\operatorname{Gc}(f,\epsilon) = 2K \cdot S = \mathcal{O}(\kappa^3 \epsilon^{-1} S), \\ &\operatorname{Gc}(g,\epsilon) = KD = \widetilde{\mathcal{O}}(\kappa^4 \epsilon^{-1}), \\ &\operatorname{JV}(g,\epsilon) = KD \cdot S = \widetilde{\mathcal{O}}(\kappa^4 \epsilon^{-1} S), \\ &\operatorname{HV}(g,\epsilon) = KD \cdot S = \widetilde{\mathcal{O}}(\kappa^4 \epsilon^{-1} S). \end{split}$$

Comparing this theorem with Theorem 5.5, we observe that the convergence rates for both scenarios are of the same order; however, the non-preference case benefits from a tighter coefficient. On the one hand, this distinction arises because the difference between MGDA and Theorem 5.4, with the former providing a tighter bound on  $d_k$ . On the other hand, the non-preference scenario can be viewed as a special case of our main theory, highlighting that the design of Equation (5) is sufficiently delicate to accommodate user preferences.

## **E** Additional numerical experiments

## E.1 Details of numerical experiments for deterministic case

All numerical experiments for deterministic case were conducted on a cluster of 4 NVIDIA H100 GPUs (96GB each) using PyTorch's DistributedDataParallel.

**Formulations.** We implement Algorithm 1 on the FC-100 dataset (Oreshkin, Rodríguez López, and Lacoste 2018) for a meta-learning task (Arnold et al. 2020; Hospedales et al. 2021) in the deterministic case. Specifically, there are m different tasks  $\mathcal{T}_i$ ,  $i \in [m]$ , each sampled from a distribution  $\mathcal{P}$ . For each task  $\mathcal{T}_i$ , we maintain a model  $\mathcal{M}(\phi, w_i)$  along with its corresponding loss function  $\mathcal{L}(\phi, w_i; \xi)$ , where  $\phi$  represents the shared parameter among all tasks,  $w_i$  is the parameter specific to task i, and  $\xi$  denotes the randomness from the dataset. In this scenario, our MOBL problem can be formulated as follows:

$$\min_{\phi} \mathcal{L}_{\mathcal{D}}(\phi, \widetilde{w}^*) := \left[ \frac{1}{|\mathcal{D}_1|} \sum_{\xi \in \mathcal{D}_1} \mathcal{L}(\phi, w_1^*; \xi), \dots, \frac{1}{|\mathcal{D}_m|} \sum_{\xi \in \mathcal{D}_m} \mathcal{L}(\phi, w_m^*; \xi) \right]$$
s.t.  $\widetilde{w}^* = \arg\min_{\widetilde{w}} \mathcal{L}_{\mathcal{S}}(\phi, \widetilde{w}) := \frac{1}{m} \sum_{i=1}^m \frac{1}{|\mathcal{S}_i|} \sum_{\xi \in \mathcal{S}_i} \mathcal{L}(\phi, w_i; \xi) + \mathcal{R}(w_i),$ 

$$(47)$$

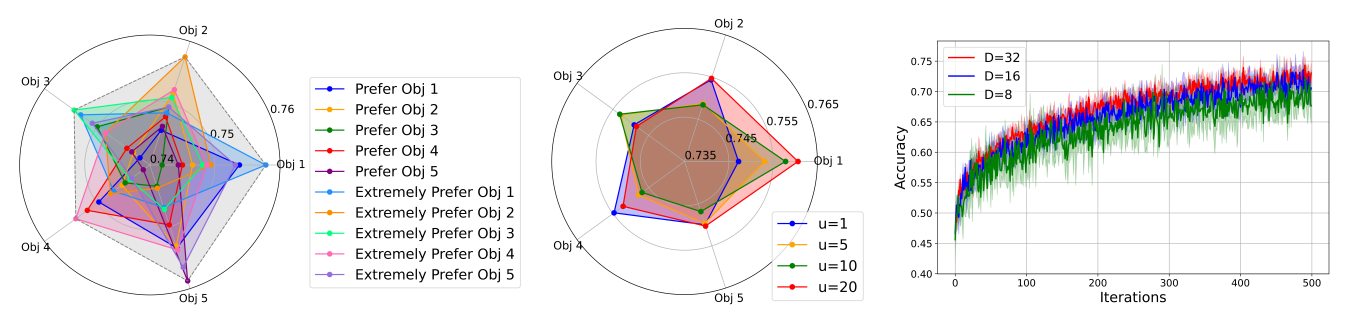
where (1)  $\widetilde{w} = [w_1, \dots, w_m]^\top$ , (2)  $\mathcal{R}(w_i)$  is a regularizer to ensure the strong convexity of the lower-level objective function, and (3)  $\mathcal{S} = \{\mathcal{S}_i\}_{i \in [m]}$  and  $\mathcal{D} = \{\mathcal{D}_i\}_{i \in [m]}$  are training datasets and test datasets, respectively. In this formulation, on the one hand, the lower-level minimizes the averaged loss function to determine the optimal task-specific parameters  $\widetilde{w}$  given the current shared parameter  $\phi$ . On the other hand, the upper-level treats the m tasks as m potentially conflicting objectives and seeks the Pareto optimal shared parameter  $\phi$  based on the output  $\widetilde{w}^*$  from the lower level.

**Datasets.** FC-100 (Fewshot-CIFAR-100) dataset is a variant of CIFAR-100 dataset (Krizhevsky, Hinton et al. 2009). The CIFAR-100 dataset contains 100 image classes, each with 500 training images and 100 test images, all of size  $32 \times 32 \times 3$ . The FC-100 dataset divides these 100 classes into 60 for training, 20 for validation, and 20 for testing. These small size sub-datasets make it more challenging for learning.

**Settings.** We consider a 5-way 5-shot meta-learning task, meaning there are m=5 tasks, and each support set contains  $|\mathcal{S}_i|=5, \forall i\in[m]$  samples. Inspired by (Ji, Yang, and Liang 2021),  $\mathcal{M}(\phi,w_i)$  is chosen to be a 4-layer Convolutional Neural Network (CNN) equipped with batch normalization, ReLU activation,  $2\times 2$  max pooling, and 64 filters in each convolutional layer for each  $i\in[m]$ . Besides, in the previous formulation, we choose Cross-Entropy as our loss function  $\mathcal{L}$ , and  $l_2$  regularizer as our regularizer  $\mathcal{R}$ .

To implement Algorithm 1 with Neumann-series approximation, we set  $S=5, K=500, D=32, \alpha=0.1, \beta=0.1, u=10,$  and  $r=[0.8,0.05,0.05,0.05,0.05,0.05]^{\top}$  as our default experiment settings. Each experiment is repeated 4 times, as we observe that fluctuations between different random seeds are minimal. To perform the ablation study, we vary several parameters as follows:

- We set different preference vectors r. Since  $r \in \mathbb{R}^{S}_{++}$  and  $\mathbf{1}^{\top}r = 1$ , we select one of the five elements of r as 0.8, while the remaining elements are set to 0.05 to represent user preferences. Therefore, for 5 different vectors r, each of them focuses on one objective.
- We set different trade-off controller constants u in Equation (5) from the set  $\{1, 10, 20\}$ . Note that a larger u places greater emphasis on the preference matching issue.
- We set different inner-loop iteration counts D from the set  $\{8, 16, 32\}$ . While the outer-loop iteration count K is fixed, this setup allows us to observe the convergence rate under different values of D.



- (a) Exploration of Pareto front under the guidance of (b) Performance under different (c) Convergence rate when prefer objective 1 different preference vectors r.
  - constant u.
- and u=10.

Figure 4: Performances of Algorithm 1.

**Additional Results.** The following simulation results further verify the effectiveness of Algorithm 1 and the correctness of Theorem 5.5. In addition to the aforementioned ablation studies, we also present the numerical results for Section D.5, where the convergence process is not guided by any user preference r.

Fig. 4a shows how Algorithm 1 converges to preference-guided Pareto stationary points. We can see that the accuracy of the more preferred objective is consistently higher than those less preferred objectives. Moreover, for those extremely preferred objectives, this trend becomes more pronounced. The outer gray area demonstrates that our WC-MHGD algorithm effectively explore a large Pareto stationarity footprint. With the preference vector  $r = [0.96, 0.01, 0.01, 0.01, 0.01]^{\mathsf{T}}$ , Fig. 4b shows the accuracy results with varying trade-off parameters u chosen from 1, 5, 10, 20. We can see that a larger u-value leads to improved performance on the extremely preferred objective 1, which confirms our theoretical insights of Equation (5). Fig. 4c shows the convergence of Algorithm 1's accuracy. We vary the inner-loop iteration count D to examine its impact on the performance of Algorithm 1. According to Theorem 5.5, a larger D results in faster convergence, which is verified in Fig. 4c.

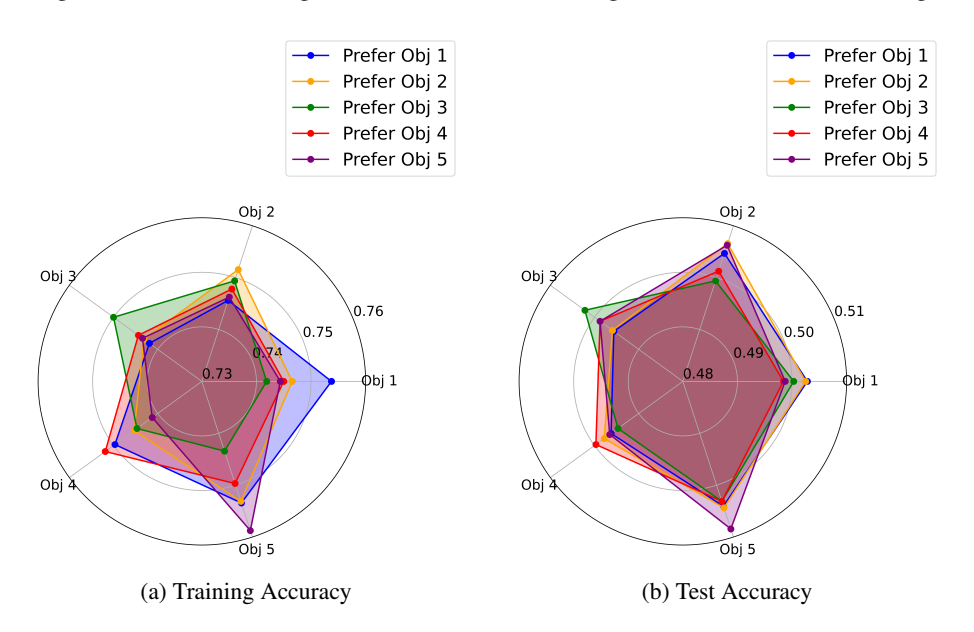


Figure 5: The accuracy with different preference vector r.

Figure 5 clearly illustrates how Algorithm 1 converges under the guidance of different preference vectors r. Since we assign one of the five objectives as the preferred objective with a value of 0.8 in each r, while the others are set to 0.05, both Figure 5a and Figure 5b essentially align with the expectations. In other words, the accuracy of objective i is almost always the highest (or at least nearly the highest) when the corresponding  $r_i = 0.8$  is the highest.

Figure 6 illustrates how the trade-off controller constant u affects the performance of Algorithm 1. As discussed in Section 4.2, a larger u places more emphasis on the preference, which is  $r = [0.8, 0.05, 0.05, 0.05, 0.05]^{\top}$  in this case. In other words, the red curve in Figure 6 is expected to achieve the highest accuracy for objective 1, as its corresponding preference value of 0.8 is the largest. Figure 6b aligns perfectly with this expectation, as larger values of u result in higher accuracy for objective 1.

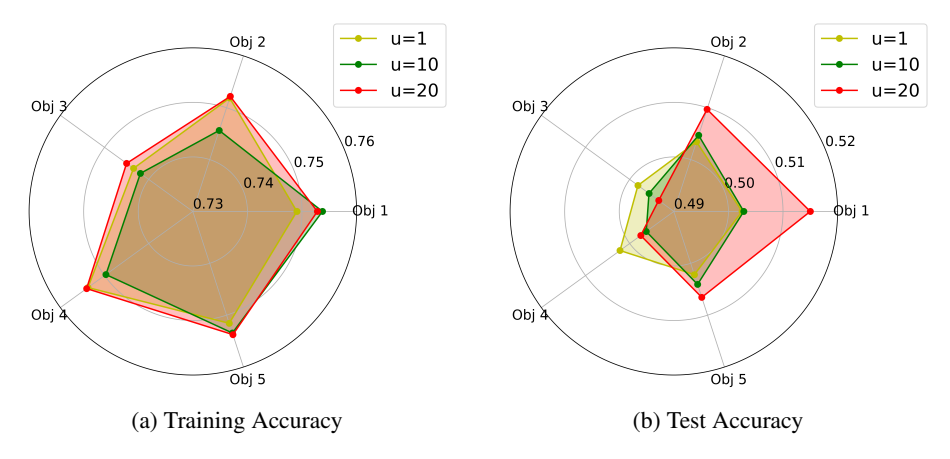


Figure 6: The accuracy with different constant u.

On the other hand, Figure 6a appears to deviate from the aforementioned expectations. However, we argue that Figure 6a is still consistent with our theory for the following reasons: (1) Since a larger u in Equation (5) places greater emphasis on the preference, the performances for objective 1 when u is set to 10 and 20 are indeed better than those when u=1. (2) Although a larger u makes the convergence process more guided by preference r, even when u is small, the convergence sequence, even if itself is not overly influenced by the preferences, can still potentially fall on any point along the Pareto front, including those guided by the preferences. Considering that the performance of objective 1 shows little difference between u=10 and u=20, we can conclude that both cases are aligned with the preference vector r to some extent. Therefore, this observation further supports the validity of our theory.

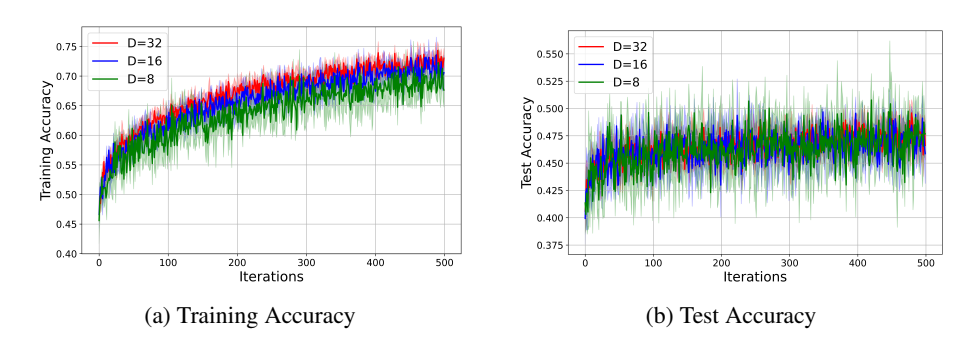


Figure 7: The average accuracy with inner iteration times D.

Figure 7 demonstrates that, given the same number of outer-loop iterations, a larger D results in higher average accuracy. This observation verifies the result in Theorem 5.5, where D acts as the exponent of  $1 - \alpha \mu_g$ , which converges to 0 as D approaches infinity. Additionally, we include standard error bars, which reveal that smaller values of D lead to greater fluctuations. This aligns with intuition: since insufficient inner-loop iterations fail to accurately determine  $y^*$ , the process is more susceptible to randomness, resulting in more pronounced oscillations. Finally, it is also worth mentioning that the low accuracies in Figure 7b is due to the few sample nature of meta-learning tasks.

Figure 8 validates the results in Section D.5, showing that the sequence arbitrarily converges to some Pareto stationary point without the guidance of any preference vector r. In contrast to Figure 5, where the accuracies in both training and testing consistently exhibit stronger performance for the objective corresponding to  $r_{\text{max}}$ , Figure 8 obviously suffers from greater randomness. In other words, the better performance for some objective in training process does not directly imply the similar results in test process. This further highlights the significance of the delicately designed approach in Section 4 for effectively addressing user preferences.

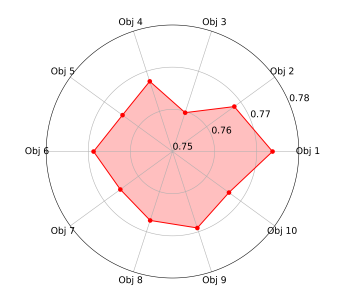
As for the baselines (Ye et al. 2021, 2024), we also enumerate the setup as follows. 1) For MOML (Ye et al. 2021), the parameters are identical to those in our default setting, as Algorithm 1 encompasses all of its required parameters. 2) For FORUM (Ye et al. 2024), we set  $\rho=2$  and  $\beta_k=\frac{1}{2k}$ , with all other parameters matching those in our setup. Notably, we also tested their recommended values ( $\rho\in\{0.5,0.7,0.9\}$ ), however,  $\rho=2$  yields the best performances.



(a) Training Accuracy for 5 objectives



(b) Test Accuracy for 5 objectives



(c) Training Accuracy for 10 objectives



(d) Test Accuracy for 10 objectives

Figure 8: The accuracy without guidance of preference vector r for 5 and 10 objectives.

#### **E.2** Details of numerical experiments for stochastic case

All numerical experiments for stochastic case were conducted on a MacBook Pro equipped with an Apple M2 Pro chip, featuring a 8-core CPU, and 16GB of memory.

Formulations. We implement Algorithm 2 on the MNIST dataset (LeCun et al. 1998) for a data hyper-cleaning task (Franceschi et al. 2018; Shaban et al. 2019) to verify the theoretical results of Algorithm 2 in the stochastic case. The objective of the data hyper-cleaning task is to train a classifier using corrupted data under a specified corruption rate p, where each label has a probability of p of being incorrect. We consider m tasks under different corruption rates p. Each task  $i \in [m]$  aims to train a model  $\mathcal{M}_{w_i}$ , parameterized by  $w_i$ . Additionally, all m tasks share the same regularization parameter  $\lambda$  and aim to minimize the validation loss. Since there are m potentially conflicting tasks, along with the complex interactions between the training and validation processes, this problem can be formulated as an MOBL problem as follows:

$$\min_{\lambda} \mathcal{L}_{\mathcal{D}}(\lambda, \widetilde{w}^*) := \left[ \frac{1}{|\mathcal{D}_1|} \sum_{(x_j, y_j) \in \mathcal{D}_1} \mathcal{L}(\mathcal{M}_{w_1}(x_j), y_j), \dots, \frac{1}{|\mathcal{D}_m|} \sum_{(x_j, y_j) \in \mathcal{D}_m} \mathcal{L}(\mathcal{M}_{w_m}(x_j), y_j) \right]$$
s.t.  $\widetilde{w}^* = \arg\min_{\widetilde{w}} \mathcal{L}_{\mathcal{S}}(\lambda, \widetilde{w}) := \frac{1}{m} \sum_{i=1}^m \frac{1}{|\mathcal{S}_i|} \sum_{(x_j, y_j) \in \mathcal{S}_i} \sigma(\lambda_j) \mathcal{L}(\mathcal{M}_{w_i}(x_j), y_j) + \mathcal{R}(w_i),$ 

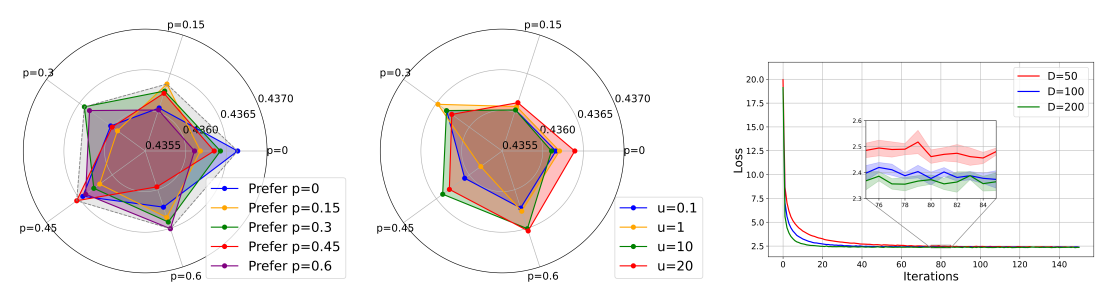
$$(48)$$

where (1)  $\widetilde{w} = [w_1, \dots, w_m]^\top$ , (2)  $\mathcal{R}(w_i)$  is a regularizer to ensure the strong convexity of the lower-level objective function, (3)  $\mathcal{S} = \{\mathcal{S}_i\}_{i \in [m]}$  and  $\mathcal{D} = \{\mathcal{D}_i\}_{i \in [m]}$  are task-specific training datasets and validation datasets, respectively, and (4)  $\sigma(\lambda)$  the sigmoid function applied on  $\lambda$ . The lower-level of this formulation finds the optimal task-specific parameters  $\widetilde{w}$  given current regularizer  $\lambda$ , while the upper-level updates this  $\lambda$  based on the output  $\widetilde{w}^*$ .

**Datasets.** We conduct our experiments on MNIST (LeCun et al. 1998), one of the most widely used datasets in the community. MNIST consists of 60,000 training images and 10,000 test images of handwritten digits, each with a size of  $28 \times 28 \times 1$ . To align with established settings, we use a subset of MNIST inspired by (Shaban et al. 2019), which includes 20,000 training images, 5,000 validation images, and 10,000 test images.

Settings. We mainly consider m=5, and the corresponding corruption rates are [0,0.15,0.3,0.45,0.6]. We choose  $\mathcal{M}_{w_i}$  to be a vector,  $\mathcal{L}$  to be Cross-Entropy,  $R(w_i)=0.1\|w_i\|^2, \forall i\in[m]$ . To implement Algorithm 2, we set S=5, (K,D)=(150,200),  $\alpha=0.1, \beta=0.1, \eta=0.5, Q=3, u=10$ , and  $r=[0.025,0.025,0.025,0.025,0.025,0.9]^{\top}$  as our default experiment settings. Each experiment is repeated 5 times. It is worth mentioning that we consider the metric 1/L, where L is the upper-level loss value defined in Equation (48). Therefore, consistent with the accuracy metric in Sections E.1 and 6, a larger covered area indicates a greater extent of exploration by the algorithm. In this section, we provide the following numerical results:

- Similarly to Section 6, we demonstrate how Algorithm 2 systematically explores the Pareto front under different preference vectors r, and how different constants u impact the performance of Algorithm 2.
- As discussed in Section D.5, the non-preference scenario can be viewed as a special case of our MOBL theory, for which we provide a theoretical analysis of the deterministic algorithm. We also note that the stochastic case shares the same underlying insight, and we present corresponding numerical results in this section.
- We also provide the numerical comparison between our approach and the MoCo method (Fernando et al. 2022).



- (a) Exploration of Pareto front under different preference vectors r.
- (b) Performance under different constant *u*.
- (c) Convergence rate when prefer objective p = 0.6 and u = 10.

Figure 9: Performances of Algorithm 2.

**Numerical Results.** The following simulation results verify the effectiveness of Algorithm 2 and the correctness of Theorem 5.7.

Figure 9a demonstrates that the design of Algorithm 2 effectively enables systematic exploration of the Pareto front under different preference vectors. Specifically, we set  $r_p = 0.9$  and  $r_{p'} = 0.025$ ,  $\forall p' \neq p$  to represent a preference for the task with corruption rate p. Consistent with Figure 1, when the preference vector favors the task with corruption rate p, our algorithm reaches the smallest loss, equivalently, the largest 1/L, on the corresponding axis. Additionally, the gray dotted curves highlight that the exploration area is significantly larger than that of any single preference-fixed curve, effectively showcasing the capability of Algorithm 2 to explore the Pareto front comprehensively.

In Figure 9b, we fix  $r = [0.025, 0.025, 0.025, 0.025, 0.025, 0.09]^{\top}$ , indicating a strong focus on the task with a corruption rate of p = 0.6, and vary the trade-off controller constant u from set  $\{0.1, 1, 10, 20\}$ . As expected, the metric 1/L increases with larger u, demonstrating a stronger emphasis on the preferred task. This result validates the theoretical insight of Equation (5), where a larger u enhances the alignment with the specified preference vector.

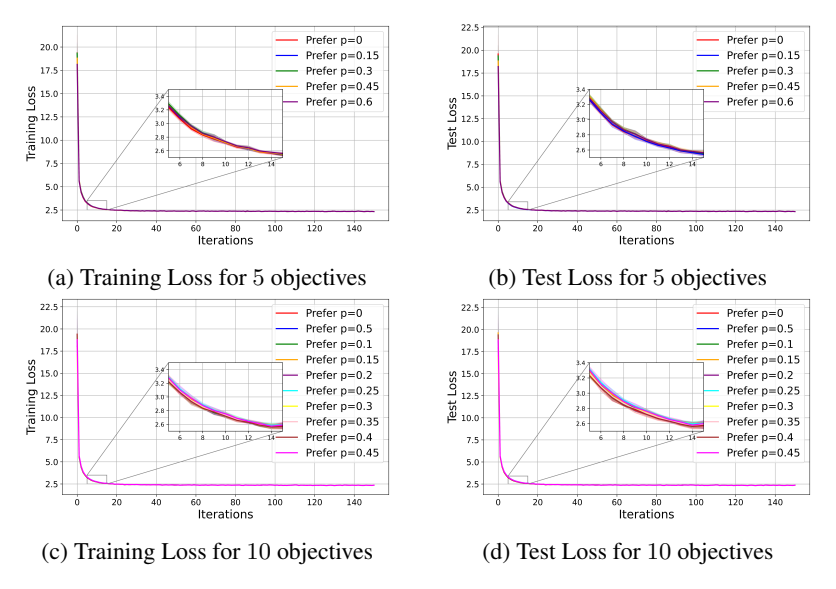


Figure 10: The average loss of 5 and 10 objectives without the guidance of preference.

Figure 9c fixes  $r = [0.025, 0.025, 0.025, 0.025, 0.025, 0.09]^{\top}$  and u = 10, while varying the inner-loop iteration count D from  $\{50, 100, 200\}$ , and shows the average loss value of 5 aforementioned potentially conflicting tasks. All three curves illustrate

their respective convergence behaviors. As implied by Theorem 5.7, D serves as the exponent of  $\frac{L-\mu_g}{L+\mu_g}$ , which is strictly less than 1. Consequently, a larger D is expected to result in a smaller loss value, and this trend is precisely reflected in the numerical results shown in Figure 9c.

Figure 10 illustrates the convergence behavior of Algorithm 4, where no preference vector is used for guidance. In this scenario, the sequence converges arbitrarily to a point on the Pareto front. We consider cases with S=5 and S=10 different corruption rates p, respectively. In both settings, the loss values converge in fewer than K=150 iterations.



Figure 11: The average performance 1/L of 5 and 10 objectives without the guidance of preference.

Figure 11 depicts the metric 1/L for each task with corruption rate p the scenarios of S=5 and S=10. Similar to Figure 8, the results indicate a random convergence pattern, meaning no single objective consistently dominates the others. This further emphasizes the effectiveness of our algorithm design in Algorithm 2, as it successfully focuses on specific objectives and achieves better performance for those objectives.

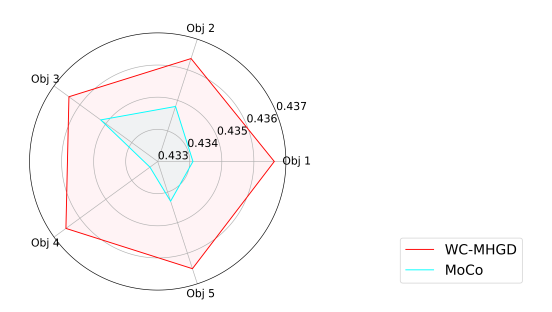


Figure 12: Comparison with baseline MoCo.

Figure 12 further demonstrates that our method consistently outperforms the baseline MoCo (Fernando et al. 2022) across all 5 objectives. This, reaffirms the effectiveness of our algorithm in systematically exploring the Pareto front.